INVITED PAPER

# Deep-Space Optical Communications: Future Perspectives and Applications

*Current technologies available for deep-space optical data transmission and networking are discussed in this paper, as well as ongoing experiments, future perspectives, and applications.*

By Hamid Hemmati, *Senior Member IEEE*, Abhijit Biswas, and Ivan B. Djordjevic, *Senior Member IEEE*

**ABSTRACT** | The concept of deep-space optical communications was formulated shortly after the invention of lasers. The promise of laser communications, high data rate delivery with significantly reduced aperture size for the flight terminal, led to the pursuit of several successful experiments from Earth orbit and provided the incentive for further demonstrations to extend the range to deep space. This paper is aimed at presenting an overview of the current status of optical communications with an emphasis on deep space. Future perspectives and applications of optical communications related to near-Earth and interplanetary communications are also addressed.

**KEYWORDS** | Deep-space optical communications; laser communications; lasers; photon-counting detectors

## I. INTRODUCTION

The ever increasing demand for returning larger volumes of data from space has been satisfied by migrating to telecommunication systems using higher electromagnetic frequencies [1]. The natural progression of increasing radio-frequency (RF) bands (S, X, and Ka) that can be efficiently transmitted through the Earth's atmosphere have been implemented for both near-Earth and deep-space telecommunications. Inherent beam-width and spectrum allocation restrictions of these bands limit further significant expansion of data return capacity. At the same time the demand for higher data-return capacity will continue for both near-Earth and deep-space missions. Higher fidelity optical and synthetic aperture radar (SAR) imaging of the Earth and planets and the support of human missions drives this demand [2], [3]. Studies concluded to date have recognized that the next major leap in expanding capacity is achievable by migrating to the significantly higher optical frequencies [4]–[7]. The key advantages of optical communications systems stem from the narrow laser beam divergence that can provide 10–100 times higher data rates with lower size, mass, and power flight systems. Furthermore, unrestricted spectrum with a few orders of magnitude bandwidth expansion (tens of terahertz at optical versus hundreds of megahertz in the RF) becomes accessible.

Ever since the discovery of lasers in the early 1960s, the use of optical frequencies for communications has been pursued. Since that time, advances in lasers, detectors, sensors, optics, and electronics have resulted in a number of successful demonstrations of optical systems [8]–[14]. These are summarized in Table 1 and include laser communication (lasercom) links from space-to-ground, space-to-space, and space-to-air demonstrations. In all cases, the space terminals have been on near-Earth orbiting platforms. Space-to-ground demonstrations have included optical links to spacecraft in: geosynchronous transfer orbit (GTO), low-Earth orbit (LEO), and geostationary-orbit

Manuscript received October 21, 2010; revised April 27, 2011; accepted June 18, 2011. Date of publication August 15, 2011; date of current version October 19, 2011. The research described in this paper was carried out at the Jet Propulsion Laboratory, California Institute of Technology under a Contract with the National Aeronautics and Space Administration. It was also supported in part by the National Science Foundation (NSF) under Grants CCF-0952711 and ECCS-0725405.

**H. Hemmati** and **A. Biswas** are with the Optical Communications Group, Jet Propulsion Laboratory, California Institute of Technology, Pasadena, CA 91109 USA (e-mail: hhemmati@jpl.nasa.gov; abiswas@jpl.nasa.gov).

**I. B. Djordjevic** is with the Department of Electrical and Computer Engineering, University of Arizona, Tucson, AZ 85721 USA (e-mail: ivan@ece.arizona.edu).

Digital Object Identifier: 10.1109/JPROC.2011.2160609

Table 1 Summary of Key Successful Demonstrations From Space

| Year | Project | Link | Rate (Gb/s) | Note |
|---|---|---|---|---|
| 1995 | LCE | GTO-to-Ground | 0.001 | JAXA |
| 2001 | GeoLITE | GEO-to-Ground | >1 | USA |
| 2001 | SILEX | LEO-GEO | 0.05 | ESA |
| 2002 | ALEX | GEO-Air | >1 | USA |
| 2005 | LUCE | LEO-GEO<br>LEO-Ground | 0.05 | JAXA |
| 2006 | LOLA | GEO-Aircraft | 0.05 | France |
| 2008 | LCTSX | LEO-LEO | 5.6 | Germany |

(GEO). Space-to-space demonstrations have included bidirectional LEO-to-GEO and most recently a project called LCTSX demonstrated 5.6-Gb/s communications link between two LEO platforms [14]. All these successful optical link demonstrations from near-Earth distances have cleared the path toward the development of operational optical communication systems for LEO and GEO spacecraft.

Note that all the links demonstrated today are from near-Earth orbit as opposed to deep space. Deep space for our present discussion is considered to be distances beyond the Moon, though the International telecommunications Union (ITU) defines deep-space as beyond 2 million kilometers. Relative to near-Earth, lasercom from deep space presents link difficulty that increases as the square of the link distance. For example, factors of 60–80-dB additional gain will be required from Mars distances relative to GEO. A mere scaling of near-Earth lasercom systems to overcome the increased difficulty will prove insufficient. Instead, new technologies and strategies for increasing the bits per photon (PPB) received with efficient lasers, detectors, and signaling (modulation and coding) are required. Furthermore, validation of these techniques through system-level demonstrations will be required prior to infusion into a future operational capability.

The National Aeronautics and Space Administration (NASA) has been pursuing research and development toward deep-space lasercom demonstrations for the past three decades. In 1992, a NASA/Jet Propulsion Laboratory (JPL) project called GOPEX successfully demonstrated laser beam pointing from two locations on the ground to the Galileo spacecraft at 6 million km [15]. In 2005, a NASA/Goddard Space Flight Center (GSFC) used the Mercury Laser Altimeter (MLA) onboard the MESSENGER spacecraft to successfully demonstrate laser beam pointing to and from Earth at ranges of 24 million km [16]. In 2003, teams from Massachusetts Institute of Technology Lincoln Laboratory (MIT-LL), JPL, and GSFC embarked on the development of the first-ever interplanetary end-to-end lasercom link between the Mars Telecommunication Orbiter (MTO) in areostationary orbit around Mars and Earth. This project, called Mars Laser Communications Demonstration (MLCD) [17], completed the preliminary system design to downlink 30 Mb/s from the nearest Mars–Earth range of approximately 0.7 AU. MLCD was terminated in 2005 due to cancellation of MTO [18].

This paper describes lasercom with an emphasis on deep-space requirements and drivers. Certain differences between near-Earth and deep-space lasercom will be pointed out and future perspectives will be discussed. The paper is organized as follows. In Section II, we summarize considerations for operating different types of space optical communication links and conclude this section with some discussions of the link equation. In Section III, we present a discussion on the signaling used, with an emphasis on deep-space links. In Section IV, we present a high-level discussion on optical systems and functions. Section V discusses future perspectives with a conclusion in Section VI.

## II. OPTICAL COMMUNICATION LINKS

Operational considerations largely dictate key requirements for designing viable, cost-effective space lasercom services. An overview of viable space lasercom links is illustrated in Fig. 1. Each link encounters different operating conditions, consequently, the system designs and technologies required to implement these designs differ. We broadly categorize these as near-Earth and deep-space links and describe them below.

### A. Near-Earth Links

For "near-Earth," we adopt LEO, medium-Earth orbit (MEO), GEO, and lunar optical links. The red double-headed arrows in Fig. 1 show optical links between spacecraft at these destinations and ground-based Earth stations. Approximately 1–2-m diameter ground telescopes are needed to receive the high-rate downlink from these distances [12], [19]–[21]. Near-Earth links use a laser beacon transmitted from the intended target receiver as a reference for acquisition, tracking, and pointing. The distances and corresponding round-trip light times are relatively short. Consequently, link acquisition uses an approach with stepped reduction of spatial uncertainty. Either spiral scans or "squinting" operations have been employed. Both direct and coherent detection [22] links have been demonstrated in space-to-space links whereas most space-to-ground links have used direct detection. Space-to-ground links coherently detected to selected ground sites have also been demonstrated [23]. Near-Earth links have supported high data rates $>$ 1 Gb/s from space-to-ground and 5.6 Gb/s in space-to-space and ground-to-space links. Near-infrared wavelength lasers at discrete wavelengths around 800, 1064, and 1550 nm have been used.

Daytime sky radiance and upwelling radiance, as well as stray light when pointing close to the Sun, contribute to additive background noise for direct detection lasercom links. Lunar links, because of the Earth–Moon geometry, encounter monthly occurrences of small angular separations from the Sun. During this condition (lasting

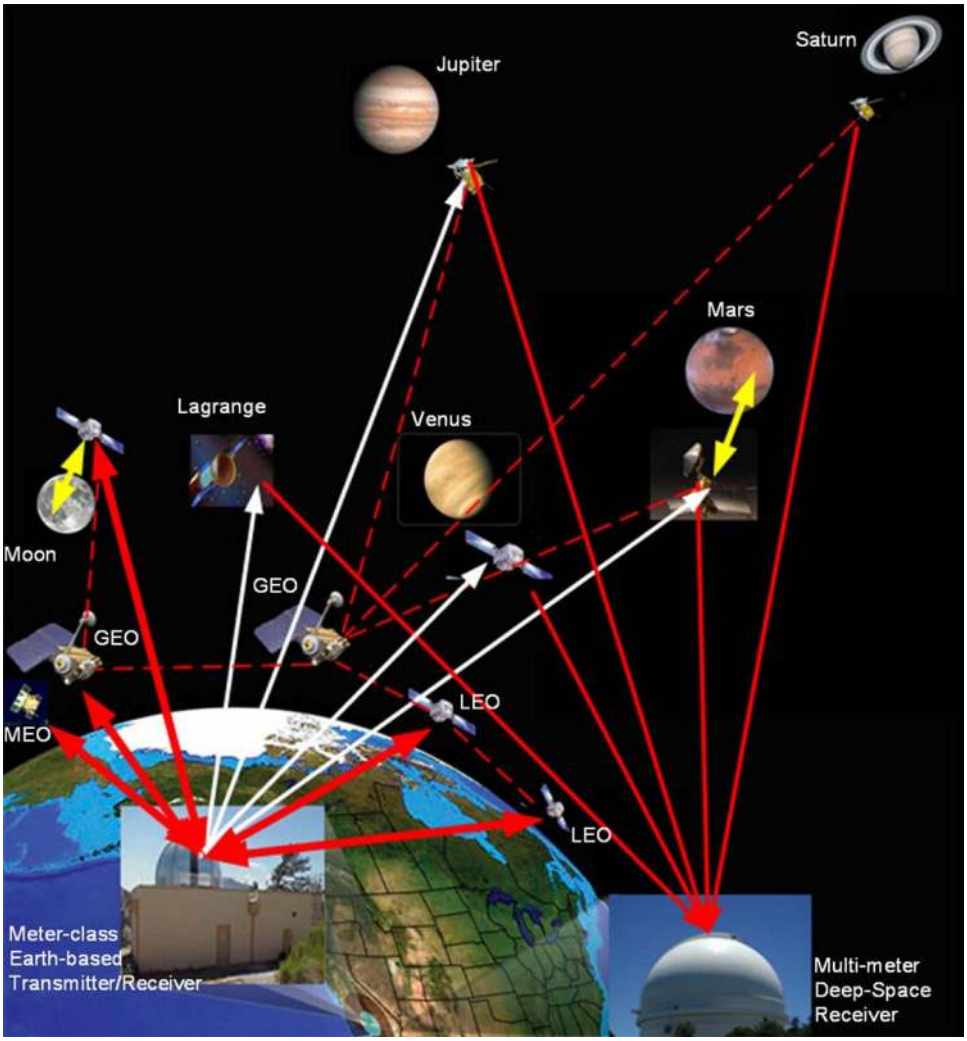


**Fig. 1.** ***A pictorial summary of different types of space optical links including multimeter diameter (large), diameter telescopes for receiving deep-space downlink, and meter-class telescopes for near-Earth bidirectional communications and transmitting beacon lasers and uplink to deep space.***

for a day or two), either the lunar optical terminal or the ground telescope has to point close to the Sun. Pointing close to the Sun is a formidable challenge for both space- and ground-based terminals. First, the optics and sensors must be protected from damage due to direct solar illumination, and second, large amounts of scattered or stray background light must be managed so that the detectors and sensors are not saturated.

### B. Deep-Space Links

Optical links from "deep space" that extend from the Sun–Earth Lagrange points [24] (approximately 0.01 AU) to planetary distances out to Saturn are shown as unidirectional red arrows (space-to-ground) and white arrows (ground-to-space) in Fig. 1. The increased deep-space distances dictate the following new link considerations: 1) increasing the isotropically radiated power (EIRP) from space, with higher power lasers and larger diameter transmitting optics; 2) transmitting lasers from the ground to the deep-space terminals, first, as a beacon for acquisition, tracking and pointing, and second, for sending uplink and possibly ranging data; 3) using larger effective diameter telescopes for collecting deep-space downlink signal on the ground; and 4) implementing signaling and detection schemes that maximize the bits/photon so that information can be transferred using faint laser signals from space.

Increasing the optical transmitting aperture diameter ($D_{\text{tx}}$) for achieving larger EIRP implies narrower beam divergence ($\propto \lambda_{\text{laser}}/D_{tx}$, $\lambda_{\text{laser}}$ being the transmitted laser wavelength from space) making downlink beam pointing requirements tighter. Furthermore, long light times corresponding to the increased distance prevent the use of interactive, stepped, near-Earth acquisition strategies. A

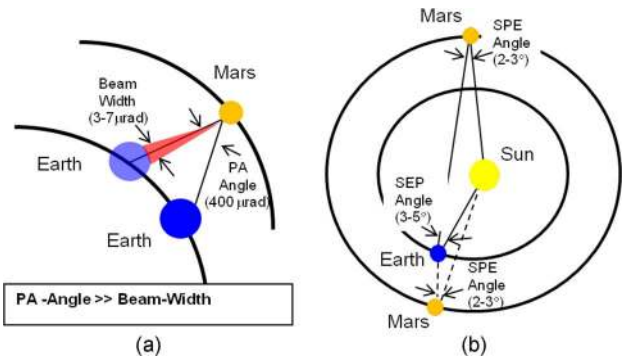


**Fig. 2.** *(a) Point-ahead (PA) angle needed to return a signal to Earth from Mars in response to a signal received from Earth. (b) Earth–Mars geometry when Sun–Earth–Probe (SEP) angles and Sun–Probe–Earth (SPE) angles are small at opposition and the SPE angle is small at conjunction.*

single step acquisition followed by tracking becomes necessary.

Deep-space spacecraft observed from ground-based receiving stations at Earth exhibit larger transverse velocities ($v_{\text{transverse}}$) and range rates ($v_{\text{range}}$), compared to near-Earth spacecraft [25]. As a result, the point-ahead angle, defined as $2v_{\text{transverse}}/c$ with $c$ being the speed of light, is much larger. The maximum point-ahead angle from Mars, shown in Fig. 2(a), is 387 $\mu$rad compared to 20–50 $\mu$rad for near-Earth spacecraft [26]. The deep-space range rates result in larger Doppler shifts, defined as $v_{\text{range}}/c$. For example, the Doppler shifts for a Mars mission can be 70 parts per million (ppm) compared to a few ppm for near-Earth links [25]. The 0.07–0.1-nm wavelength shifts at 1064 and 1550 nm must be accounted for when designing spectral filters for rejecting the background additive noise. The same Doppler shift can result in approximately 140-kHz frequency shift in a 2-GHz clock used for signaling.

Another distinguishing feature of deep-space links is the longer continuous durations at near-Sun angles. As an example, Fig. 2(b) shows the geometry of Earth–Sun and Mars. The Sun–Earth–Probe (SEP) and Sun–Probe–Earth (SPE) angles both get small near-superior conjunction so that both space and ground terminals have to communicate with a small angular separation to the Sun [25]. For link geometries near an inferior conjunction, the SPE can be small while the SEP angle is large so that the ground terminal views the night sky while the space terminal has to point close to the Sun. For link outages less than 1–4 weeks, SEP angles as low 3°–5° and SPE angles of 2°–4° are encountered. Smaller SEP/SPE angles with varying durations are realized for spacecraft around other planetary bodies [27]. Near-Sun operating consideration pointed out earlier in Section II-A applies for deep space; however, the larger effective aperture diameter on the ground and the extended durations present a much bigger challenge.

In the links conceptualized in Fig. 1, meter-class ground telescopes serve as receivers and transmitters for near-Earth links. For deep-space links these ground telescopes can serve as subaperture multibeam transmitters, whereas much larger effective diameter (5–12-m class) telescopes are required for receiving data rates from deep space (see Section IV-B). The use of separate transmitting and receiving apertures for deep space are preferred so that the single-photon sensitive receivers can be optically isolated from high-power deep-space transmitters discussed next.

In Fig. 1, beacon lasers from the meter-class diameter ground telescopes to all deep-space destinations are shown (white arrows). The consequences of long light-travel-time to deep-space destinations, tens of seconds to hours, were pointed out above. Additionally, with increasing distance the beacon laser from ground-based Earth stations will get dimmer. Atmospheric turbulence induced beam spreading limits the effective beam width that can be transmitted to space. Therefore, overcoming the space losses by increasing the laser power becomes prohibitive. Traditional adaptive optics techniques for correcting atmospheric degradation of ground transmitted beacons do not present obvious solutions because: 1) the point ahead is many isoplanatic angles so that using the downlink signal as a reference source will not correct anisoplanatism; and 2) the faint downlink signal will not serve as a reliable reference. Alternative solutions, such as the use of guide stars, especially during the day, need development. Thus, transmitting the laser beacon signal to deep-space distances presents a number of new challenges that are not encountered in near-Earth links. As a result, the beacon irradiance that can be delivered to space terminals in deep space is limited. Therefore, in addition to the tighter pointing requirements and the need for single step acquisition alluded to earlier, use of a dim beacon as a pointing reference is also mandated at deep-space ranges. Increased additive background noise when SPE angles are small further limits beacon-assisted acquisition, tracking, and pointing. Current studies that have analyzed beacon-assisted acquisition and tracking from Mars farthest range with SPE angles of 2°–3° using 22–30-cm diameter space terminal aperture diameters suggest this to be viable [28], [29]. In these cases, the beacon is modulated and temporal acquisition is utilized in order to discriminate against background noise (see Section IV). Beacon-assisted acquisition out to Jupiter distances has been reported [30]. However, the viability of beacon-assisted acquisition at Saturn or larger distances has not been studied, therefore, in Fig. 1 the white line representing a ground beacon is not shown. Certainly, the ability to transmit a diffraction-limited laser beam from the ground using adaptive optics or from above the Earth's atmosphere would allow extending the range of beacon-assisted acquisition beyond Jupiter. Beaconless schemes relying on the use of the Earth viewed in the infrared as a beacon [31] or the use of

high precision star trackers [30] are also schemes that have been identified and no doubt will be pursued in future studies and designs.

Special modulation schemes can be implemented on the beacon lasers for transmitting uplink data or ranging sequences. These can be an inner higher rate modulation within a slower rate outer modulation used to aid acquisition.

The large effective diameter telescopes on the ground need not be of astronomical quality with a field-of-view (FOV) of 1 $\mu$rad, however, surface quality associated with solar collectors $\sim$440-$\mu$rad FOV are unacceptable because the additive background noise from sky radiance would be excessive for photon-counting detectors. Nominally, 10–20-$\mu$rad ground telescope FOV or atmospheric "seeing" limited quality is adequate for optical communication telescopes. The large effective diameter can be achieved by using arrays of smaller diameter telescopes or a single large aperture [32], [33] and each choice has prospects and consequences.

With telescope arrays, either the photon signals can be combined prior to temporal acquisition or temporal acquisition can be performed at each aperture using a separate receiver and the synchronized signal can be combined. The uncertainties of path length difference especially when the signal-to-noise ratio is poor do not favor the first approach. The second approach is more robust but also requires the element aperture diameter to provide sufficient signal-to-noise ratio for performing acquisition. Studies indicate that an element aperture diameter of 2.5 m can satisfy link acquisition at the farthest Mars distance under nominal atmospheric conditions. However, 2.5 m is marginal under worst case atmospheric conditions and will prove inadequate for acquisition from outer planet distances [29]. On the other hand, if the unit element aperture diameter becomes larger than 2.5 m it may not prove cost effective to build arrays. Some other implementation advantages of arrays is the possibility of phasing the cost with time gradually achieving the large effective diameter, and the inherent redundancy.

Single large telescopes offer simpler operations with a single receiver and single optical path making easier calibration and alignment. As a result of atmospheric turbulence, larger apertures will result in more spatial modes at the focal plane requiring larger effective area detectors. Large telescopes may be prone to single point failures. Studies indicate that for a single telescope a segmented primary mirror [34] is more cost effective than a monolithic primary mirror.

As alluded to earlier, telescope design needs to allow near-Sun pointing for extended duration. The use of baffles to reject stray light scattered from structural parts is utilized. The use of solar protection filters at the entrance aperture has also been considered, however, the throughput of this filter and its scattering characteristics are quite stringent.

Finally, since the signals arriving from deep space are faint, link margin on the ground must be increased while avoiding undue burden on the space terminal. Some strategies for increasing photon efficiency are the use of pulse-position modulation (PPM) with photon-counting receivers on the ground. This combination can provide 10–20-dB gain over the direct detection optical preamplifier or avalanche photodiode receivers [35]. To improve the photon efficiency in addition to efficient signaling (see Section III) and detection (see Section IV) attention must be paid to the limited resources on deep-space spacecraft. This implies using ultralight-weighted optical systems to achieve larger aperture diameters and realizing highly efficient electrical to optical conversion in lasers to minimize power usage. It is worth pointing out that electrical-to-optical conversion efficiency of existing space communication near-infrared lasers is poor compared to RF transmitters. Research to overcome this limitation is needed to enhance the desired efficient implementation of optical communications from deep space.

### C. Space-to-Space Links

Space-to-space links are not vulnerable to weather or cloud outages. Moreover, diffraction-limited single-mode laser beams can be exchanged so that phase coherent techniques like heterodyne or homodyne that deliver high link capacity, without vulnerability to additive background noise (pointing close to the Sun, for example), can be implemented. Indeed the LEO-to-LEO 5.6 Gb/s [14] took advantage of this.

For returning data from deep space, orbiting receivers with large collecting apertures [37] have been studied and are depicted in Fig. 1. The main reason why these are not being considered for immediate implementation is the prohibitive cost of launching and maintaining orbiting space receivers. The cost of a single space receiver may exceed or be equivalent to that of an entire ground network. Furthermore, orbiting assets may have single points of failure. Operating links using ground-based receiver, on the other hand, will provide invaluable experience in understanding optical link operations from deep space, with opportunities for incrementally improving receiver technology. Thus, space-to-space links though compelling in terms of overcoming atmospheric and weather limitations will likely be implemented farther in the future after the basics of operating deep-space optical links have been validated and matured.

### D. Access (Proximity) Links

The bulk of data returned from recent Mars rovers and landers have been relayed back to Earth using ultrahigh-frequency (UHF) access links [38]. Optical links can also provide this service, the potential advantage being the ability to provide nearly two orders of magnitude higher data volume, with mass and power resources comparable to that used by UHF radios. The Moon and Mars are

potential destinations where this enhanced optical service could be implemented and are shown by bidirectional yellow arrows in Fig. 1. Technology challenges here are primarily in the design of optical terminals, which are deployed on the surface assets (landers and rovers) since the resource limitations are severe and furthermore the terminals have to survive the rigors of deep-space launch and landing on a planetary surface. The environment on planetary and lunar surfaces (including dust) needs to be taken into account as well. Efforts to validate the concept of operations for access links, where autonomous acquisition and tracking are required, have been emulated with airborne terminals receiving high-rate data from stationary ground terminals [39].

### E. Weather and Clouds

A key challenge faced by near-Earth and deep-space links discussed in Sections II-A and B relative to RF is the adverse weather vulnerability and blockage due to clouds. Various strategies to circumvent this weakness have been identified. One such scheme relies on a global network of ground-based receivers that, due to weather diversity, will ensure the ability to deliver data back to Earth [36]. Another scheme is to put Earth receivers in orbit above the atmosphere [37]. Either of these strategies or some combination will very likely prove to be a robust solution, as ongoing trade studies and technology development progress.

For future operational deep-space ground receiving infrastructure colocating the transmitter and the receiver in the same weather cell will be advantageous from the standpoint of minimizing link outages. However, optical link demonstrations can take advantage of existing ground assets. This approach can result in significant near term cost savings while providing a means for validating and maturing the technology, prior to operational use. As past system architectures like MLCD have shown, noncolocated ground transmitters and receivers can be used to perform deep-space lasercom demonstrations as long as the angular separation of these assets as viewed from deep space is within the terminal FOV, allowing adequate margin for point-ahead angles.

### F. Optical Link Equation

Link performance for optical downlink from space to ground can be traced to the photon budget composed of average detected signal and noise. Equations (1) and (2) quantify the signal flux ($n_s$) and the noise flux ($n_b$), in photoelectrons per second (pe/s) for direct detection optical links

$$n_s = \mathrm{EIRP}.L_{\mathrm{space}}.L_{\mathrm{atm}}.G_R.\eta_R.\eta_{\mathrm{DetEff}}\frac{\lambda_{\mathrm{laser}}}{hc}. \tag{1}$$

In (1), EIRP is defined as the product of: 1) the average laser power $P_{tx}$; 2) far-field on-axis optical antenna gain $(\pi D_{tx}/\lambda_{\mathrm{laser}})^2$ [40]; 3) the overall transmitting efficiency $\eta_{tx}$, composed of laser coupling to optics, wave-front error losses, optical transmission, and efficiency of laser beam coupling to the far field; and 4) residual pointing loss $L_{\mathrm{pointing}}$

$$\mathrm{EIRP} = P_{tx}\left(\frac{\pi^2 D_{tx}^2}{\lambda_{\mathrm{laser}}^2}\right)\eta_{tx}L_{\mathrm{pointing}}. \tag{1a}$$

$L_{\mathrm{space}}$ represents the dominant loss through free space, and $L_{\mathrm{atm}}$ is the atmospheric attenuation. $G_R$ represents the receive antenna gain and $\eta_R$ the receive photon efficiency composed of optical transmission, scattering, polarization losses, and filter transmission. Finally, $\eta_{\mathrm{DetEff}}$ is the photodetection efficiency and $h$ is Planck's constant.

For deep-space links, the $L_{\mathrm{space}}$ in (1) is huge and must be overcome by upward scaling of gains in space (EIRP) and on the ground gain ($G_R\eta_R\eta_{\mathrm{DetEff}}$). It will generally prove cost effective to burden the ground with the highest realizable gain required for overcoming $L_{\mathrm{space}}$; hence the motivation for the largest practical effective aperture diameter on the ground, as mentioned earlier and further elaborated on in Section IV-B

$$n_b = \Big[L_{\mathrm{sky,planet,stray}}.\Omega_{\mathrm{FOV}}.A_{\mathrm{recvr}}\Delta\lambda + \mathrm{UnExtLaserSignal}\Big]\eta_{\mathrm{DetEff}}\frac{\lambda_{\mathrm{laser}}}{hc} + \mathrm{DarkCounts}. \tag{2}$$

In (2), $L_{\mathrm{sky,planet,stray}}$ represents background radiance from the sky (on Earth), sunlight reflected from planetary bodies that are larger than the detector field of view, and stray light that scatters into the detector solid angle in steradians, $\Omega_{\mathrm{FOV}}$. $A_{\mathrm{recvr}}$ is the receiving aperture area and $\Delta\lambda$ is the noise-equivalent bandwidth (NEB) of the spectral filter in front of the detector. UnExtLaserSignal refers to the "in-band" residual laser power when the laser is not transmitting a pulse and DarkCounts represents detector dark noise.

The background photoelectron flux $n_b$ limits daytime link performance with increased severity as the SEP or SPE angle decreases. From (2), $n_b$ can be restricted by limiting the detector solid angle ($\Omega_{\mathrm{FOV}}$) and using narrow spectral filters ($\Delta\lambda$). However, for ground-based receivers, $\Omega_{\mathrm{FOV}}$ is proportional to the number of spatial modes collected through the atmosphere, which in turn is proportional to $(D_{rx}/r_0)^2$; $D_{rx}$ being the receiver aperture diameter and $r_0$ the atmospheric coherence length [41]. Thus, gaining signal by increasing $D_{rx}$ requires a larger solid angle, which results in an increased additive background noise. The

NEB $\Delta\lambda$ of the spectral filter is limited by technology and considerations for spectrally acquiring the signal in the presence of Doppler shifts. Receiving a circularly polarized laser beam from space is another strategy used to reduce the unpolarized background photon flux by half [33].

Predicting $n_s$ and $n_b$ using the link equation requires reliable estimates for $L_{\mathrm{atm}}$, $r_0$, and $L_{\mathrm{sky,planet,stray}}$. For a given ground site the availability of measured cumulative statistics for these atmospheric quantities allows the derivation of reasonable bounds on $n_s$ and $n_b$. In the absence of site statistics, atmospheric models can be used to estimate atmospheric parameters.

Values of $n_s$ and $n_b$ predicted by (1) and (2) to a large extent determine whether the link can be temporally acquired or synchronized. Additional parameters such as clock stability and link dynamics also limit the probability of temporal acquisition for a given signal-to-noise ratio. For near-Earth links, commercial clock and data recovery systems based on phase-locked loops, which operate with relatively higher signal-to-noise ratios, can be used. For photon-starved deep-space links, temporal acquisition is more challenging. In past designs and tests, a predetermined pattern of repetitive pulses (pilot tones) [32] or the absence of a pulse (guard-time slots) have been used to aid acquisition and synchronization [42], [43]. Robust deep-space links are designed with a low probability of missing the pilot tones or guard-time slots under the most stressing operating conditions, i.e., near-Sun pointing combined with large distances, small $r_0$, and high atmospheric attenuation.

Near-Earth and deep-space links can be supported at discrete wavelengths. Both the availability of lasers that can support high-rate communications and system considerations drive the choice of lasercom wavelengths. The latter is discussed here briefly while laser considerations are deferred to Section IV. Some of the system considerations for wavelength selection are: far-field antenna gain, transmission through the atmosphere, vulnerability to additive background noise, atmospheric turbulence, and the availability of efficient high-bandwidth detectors. Shorter wavelengths result in higher far-field gain but tighter pointing requirements. Atmospheric considerations (transmission, turbulence, and additive background) favor higher wavelengths within the allowable transmission bands [44]. An assessment of these wavelength design drivers in the context of available laser and detector components dictates the use of near-infrared wavelengths in the vicinity of 1060 and 1550 nm. Of these wavelengths, 1550 nm is superior from an atmospheric standpoint notwithstanding the higher antenna gain at 1060 nm [see (1a)]. In previous work, we have shown through link analysis the possible performance improvements that can be realized for a Mars optical communication downlink [45].

## III. SIGNALING

This section is related to the modulation and coding for deep-space optical communications. A typical digital optical communication system employing channel coding is shown in Fig. 3. As mentioned earlier, channel coding represents a key enabling technology for deep-space lasercom, and channel codes approaching Shannon's capacity within 1 dB have been recently reported [46]. Source information is generated in the form of a sequence of symbols. The channel encoder accepts these message symbols and adds redundant symbols following a prescribed encoding rule. The channel coding is the act of transforming of a length-$k$ information sequence into a length-$n$ codeword. A modulator that can impress the encoded sequence on the laser carrier in a form suitable for transmission over the optical channel follows. In direct detection systems, the photo-detector output is proportional to the incident power, meaning that the phase information is lost. Since the photo detector can distinguish only among different power levels, intensity modulation of the laser transmitter is required. The most common modulation formats for free-space optical communications [46] are ON–OFF keying (OOK), PPM, and wavelength shift keying (WSK). Because PPM is an energy-efficient modulation format, it is commonly used in deep-space communications, while OOK is suitable for near-Earth optical links.

The signal constellation for $M$-ary PPM ($M$ is the signal constellation size) is represented by $\{p(t-\tau_i)\}$ $(i \in \{1, 2, \ldots, M\})$, where $\tau_i$ is the delay parameter associated with the $i$th signal constellation point, and $p(t)$ is the pulse shape. The corresponding signal constellation for OOK is represented by $\{d_i p(t)\}$ $(i \in \{1,2\}; d_i \in \{0,1\})$, whereas the signal constellation for WSK is represented by $\{p(t, \lambda_i)\}$ $(i \in \{1, 2, \ldots, M\})$, where $\lambda_i$ is the operating wavelength of $i$th symbol. To improve the power efficiency of WSK, it can be combined with PPM, as discussed in [46]. The PPM is a very power-efficient modulation scheme but of poor spectral efficiency. To improve the spectral efficiency of PPM, the overlap PPM (OPPM) is proposed [47]. In OPPM, the symbol interval $T$ is divided into $NM$ chips, and a single pulse consists of $N$ chips resulting in

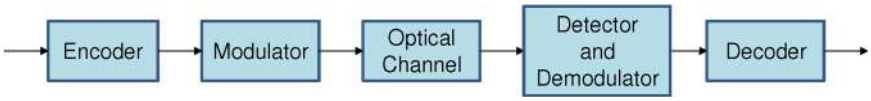


**Fig. 3.** *Block diagram of a point-to-point optical communication system.*

$\log_2(NM-1)$ bits per $T$ seconds being transmitted. Another alternative approach is based on differential PPM (DPPM) [48], also known as truncated PPM (TPPM), in which the new PPM symbol begins as soon as the slot containing the pulse is over. This scheme, however, suffers from variable-rate code design problem and catastrophic error propagation, so that PPM seems to be an only viable option for deep-space optical communication.

On the receiver side, the decoder exploits the redundant symbols inserted on the transmitter side to determine which message symbol was actually transmitted. Encoder and decoder operate as though the whole optical digital transmission system is a discrete channel. The codes commonly considered in deep-space communications belong either to the class of *block codes* or to the class of *convolutional codes*. In an $(n,k)$ *block code* the channel encoder accepts information in successive $k$-symbol blocks, and adds $n-k$ redundant symbols that are algebraically related to the $k$ message symbols; thereby producing an overall encoded block of $n$ symbols $(n>k)$, known as a *codeword*. In *convolutional code*, however, the encoding operation may be considered as the discrete-time convolution of the input sequence with the impulse response of the encoder.

As mentioned above, the channel code considers the whole transmission system as a discrete channel, in which the sizes of input and output alphabets are finite. A particular instance of this channel, a discrete memoryless channel (DMC), is characterized by the channel (transition) probabilities $\{p(y_j|x_i)\}$ $(i=1,\ldots,M; j=1,\ldots,N)$. The transition probability $p(y_j|x_i)$ represents the conditional probability that channel output $Y=y_j$ given the channel input $X=x_i$. The transition probability can be derived from statistical optical channel models by means of conditional probability density functions (pdfs) $f_{Y|X}(y|x)$. There exist several *optical channel models* for deep-space communications such as: Poisson, additive white Gaussian noise (AWGN), McIntyre–Conradi [49], Webb–McIntyre–Conradi (WMC) [50], and WMC plus AWGN channel models. For high photon-efficient deep-space links based on photon counting receiver, the Poisson channel model is the most adequate. Its pdf is given as follows:

$$f_{Y|X}(k|i)=\frac{K_i^k e^{-K_i}}{k!}, \qquad i=0,1, \qquad k=0,1,2,\ldots \quad (3)$$

where $K_i$ is the average number of photons detected when $X=i$ $(i=0,1)$. If the sizes of input and output alphabets are the same, $M=N$ and transition error probabilities are equal $p(y_j|x_i)=P_s/(M-1)$ $(j\neq i)$, where $P_s$ is the symbol error probability; the corresponding DMC is known as $M$-ary symmetric channel. If we let the size of output alphabet $N\to\infty$, the corresponding channel model is known as $M$-ary input unconstrained-output channel. The decision rule that minimizes average symbol error probability, when all input symbols are equally likely, is known as the maximum-likelihood (ML) decision rule and can be expressed in terms of log-likelihood function $L(x_i)=\log f_Y(\boldsymbol{y}|x_i)$, where $\boldsymbol{y}$ is the observation vector, as follows:

$$\text{Set } \hat{x}=x_i \text{ if } L(x_k) \text{ is maximum for } k=i. \quad (4)$$

The corresponding symbol error probability can be calculated, assuming that all symbols are equally likely, by

$$\begin{aligned} P_s &= 1-\frac{1}{M}\sum_{i=1}^{M} P(\boldsymbol{y} \text{ lies in } Z_i|x_i \text{ sent}) \\ &= 1-\frac{1}{M}\sum_{i=1}^{M}\int_{Z_i} f_Y(y|x_i)\,dy \end{aligned} \quad (5)$$

where $Z_i$ is the decision region corresponding to the $i$th transmitted symbol. For direct detection of OOK, the corresponding ML decision rule is given by

$$\hat{x}=\begin{cases} 1, L(y)<0 \\ 0, L(y)\geq 0 \end{cases}; \quad L(y)=\log\left[f_{Y|X}(y|0)/f_{Y|X}(y|1)\right] \quad (6)$$

where $L(y)$ is known as the log-likelihood ratio (LLR).

We define $K_s\approx Mn_s\tau_s$ and $K_b=n_b\tau_s$ to denote the number of signal and background photoelectrons per slot with $\tau_s$ representing the slot width. The bit error rate (BER) plots for the Poisson channel for different background radiations $K_b$ are shown in Fig. 4(a). In Fig. 4(b), we show uncoded BERs of PPM over a Poisson optical channel for different number of slots in the presence of background radiation for $K_b=1$. These results are obtained based on corresponding expressions given in the Appendix. The power efficiency can be improved by increasing the number of slots $M$, however, the corresponding channel capacity decreases with $M$ so that proper engineering is needed in practice.

One important figure of merit for optical channel is the *channel capacity*, which is obtained by maximization of mutual information over all possible input distributions

$$C=\max_{\{p(x_i)\}} I(\boldsymbol{X};\boldsymbol{Y}),\ I(\boldsymbol{X};\boldsymbol{Y})=H(\boldsymbol{X})-H(\boldsymbol{X}|\boldsymbol{Y}) \quad (7)$$

where $H(\mathbf{U})=E(\log_2 P(\boldsymbol{U}))$ denotes the entropy of a random variable $\boldsymbol{U}$ and $E(\cdot)$ denotes the mathematical expectation operator. Since for $M$-ary input $M$-ary output symmetric channel, such as $M$-ary PPM,

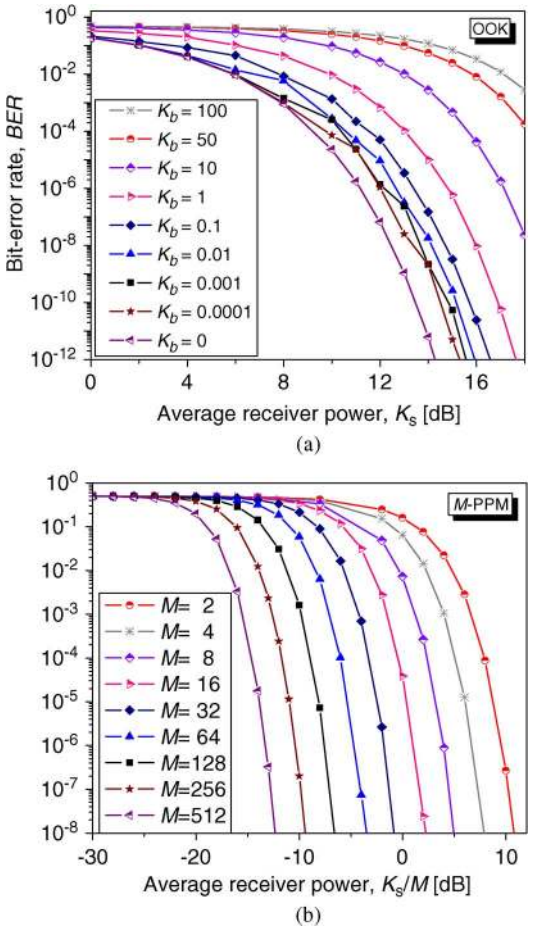


**Fig. 4.** ***Poisson channel uncoded BERs for: (a) OOK, (b) M-ary PPM for $K_b = 1$.***

$p(y_j|x_i) = P_s/(M-1)$ and $p(y_j|x_j) = 1 - P_s$, the channel capacity, in bits per symbol, can be found by

$$C = \log_2 M + (1-P_s)\log_2(1-P_s) + P_s \log_2(P_s/(M-1)). \tag{8}$$

For the unrestricted output channel, the channel capacity is given by [51]

$$C = E_{Y_1,\cdots,Y_M} \log_2 \left[ \frac{M l(Y_1)}{\sum_{j=1}^{M} l(Y_j)} \right] \quad \text{[bits per symbol]} \tag{9}$$

where $l(y) = f_{Y|X}(y|1)/f_{Y|X}(y|0)$ and distribution of $Y_j$ is $f_{Y|X}(y|0)$ for $j > 1$. The $M$-fold integration is intractable when numerical integration is used, but still feasible with Monte Carlo integration. For Poisson channel in the presence of background integration, (9) becomes

$$C = \log_2(M)\left\{1 - \frac{1}{\log_2 M} E_{Y_1,\cdots,Y_M} \log_2 \left[ \sum_{i=1}^{M} \left(1 + \frac{K_s}{K_b}\right)^{Y_j - Y_1} \right] \right\} \tag{10}$$

[51] which in the absence of background radiation is simply

$$C = \log_2(M)(1 - e^{-K_s}) \quad \text{[bits per symbol]}. \tag{11}$$

The channel capacity represents an important bound on data rates achievable by any modulation and coding schemes. It can also be used in comparison of different coded modulation schemes in terms of their distance to the channel capacity curve. In Fig. 5, we show the channel capacity for Poisson $M$-ary PPM channel against the average number of signal photons per slot, expressed in a decibel scale, for the average number of background photoelectrons per slot $K_b = 1$.

*The channel codes of* interest in deep-space optical communications include [46]: Reed–Solomon (RS), convolutional, turbo-like serial and parallel concatenated codes [52], and low-density parity-check (LDPC) codes [53]. The RS codes represents a special class of nonbinary Bose–Chaudhuri–Hocquenghem (BCH) codes [54]. RS codes are the most commonly used nonbinary codes.

The codeword length of RS codes is determined by $n = q - 1$ ($q$ is a prime power), so that RS codes are relatively short codes. The generator polynomial degree is $2t$ ($t$ is the error correction capability) and it is the same as the number of parity symbols $n - k = 2t$. Since the minimum distance of BCH codes is $2t + 1$, the minimum

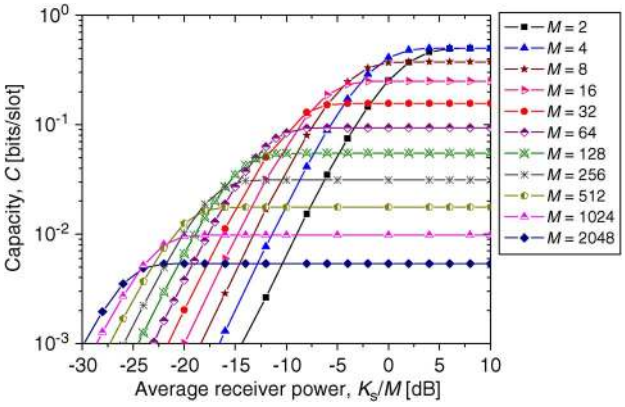


**Fig. 5.** ***Channel capacity for M-ary PPM on a Poisson channel for $K_b = 1$.***

distance of RS codes is $d_{\min} = n - k + 1$, satisfying therefore the Singleton bound ($d_{\min} \leq n - k + 1$) with equality and belonging to the class of maximum-distance separable (MDS) codes. When $q = 2^m$, the RS codes parameters are: $n = m(2^m - 1)$, $n - k = 2mt$, and $d_{\min} = 2mt + 1$. Therefore, the minimum distance of RS codes, when observed as binary codes, is large. The RS code may be considered as burst error-correcting code. This binary code is able to correct up to $t$ bursts of length $m$. Equivalently, this binary code is able to correct a single burst of length $(t-1)m + 1$.

A turbo encoder comprises the concatenation of two (or more) convolution encoders, while corresponding decoders consist of two (or more) convolutional soft decoders in which extrinsic probabilistic information is iterated back and forth among soft decoders [54]. *Parallel turbo encoder* consists of two rate 1/2 convolutional encoders arranged in parallel concatenation scheme. In a *serial turbo encoder*, the serially concatenated convolutional encoders are separated by $K/R_0$-interleaver, where $R_0$ is the code rate of outer encoder. The interleaver takes incoming block of bits and arranges them in pseudorandom fashion prior to being encoded by the second encoder, so that the same information bits are not encoded twice by the same recursive systematic convolutional (RSC) code, in case that identical RSC codes are used. Since the resulting code rate of parallel turbo encoder is low, the puncturer deletes the selected bits in order to reduce the coding overhead, and resulting code rate is $R = K/(K + P)$, where $P$ is the number of parity bits remaining after puncturing. Iterative (turbo) decoder interleaves two soft-input–soft-output (SISO) decoders, exchanging the extrinsic information iteratively and cooperatively. The role of iterative decoders is to iteratively estimate the *a posteriori* probabilities (APPs) $\Pr(u_k|\boldsymbol{y})$, where $u_k$ is $k$th data bit ($k = 1, 2, \ldots, K$), and $\boldsymbol{y}$ is a received codeword plus noise $\boldsymbol{y} = \boldsymbol{c} + \boldsymbol{n}$. For iterative decoders, each component decoder receives extrinsic or soft information for each $u_k$ from its companion decoder, which provides "the prior" information. The key idea behind extrinsic information is that decoder $D_2$ provides the soft information to $D_1$ for each $u_k$ using only information not available to $D_1$. If the parity-check matrix of a liner block code has a low density of ones and the number of ones per row and per column is constant, the code is said to be a *regular* LDPC code. Decoding of LDPC codes is based on sum–product algorithm (SPA) [54], which is an iterative decoding algorithm where extrinsic probabilities are iterated forward and back between variable and check nodes of bipartite (Tanner) graph representation of a parity-check matrix $\boldsymbol{H}$.

In Fig. 6, we show the minimum channel capacity BERs for different code rates for 64-PPM over Poisson channel in the presence of background radiation with average number of background photons of $K_b = 0.2$. The plots are obtained by employing Fano's inequality [54] and can be used as reference for different classes of codes. For example, it has been shown in [53] that for 64-PPM over Poisson channel with a serial concatenated turbo code (8184, 4092) we are about 1 dB away from channel capacity (for $K_b = 0.2$ at BER of $10^{-5}$), while with an LDPC (8192, 4096) code, of fixed column weight 6 and irregular row weight, we are 1.4 dB away from channel capacity.

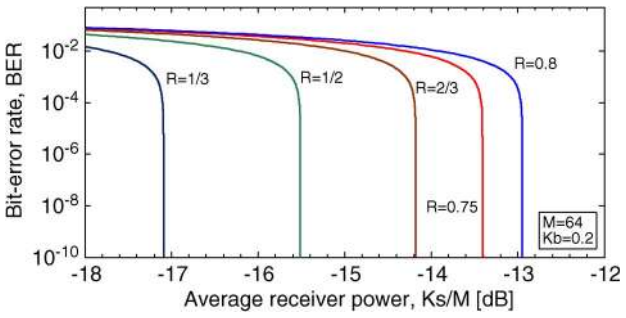


**Fig. 6.** *Channel capacity BER curves against average receiver power for 64-PPM over a Poisson channel with background radiation of $K_b = 0.2$ and different code rates.*

## IV. OPTICAL COMMUNICATION SYSTEM

### A. Flight Subsystem

Major assemblies of a lasercom flight subsystem include: 1) the laser transmitter assembly; 2) the optical telescope assembly for transmitting and receiving laser signals; 3) the acquisition tracking and pointing (ATP) assembly for acquiring the beacon signal, stabilizing the line of sight and pointing the downlink laser; and 4) the electronics assembly. A generic block diagram with these assemblies is shown in Fig. 7(a) while Fig. 7(b) shows the conceptual design of a deep-space terminal. The key functional requirements for these various flight assemblies are listed as follows.

- Laser power $P_{tx}$ is driven by the EIRP while the modulation scheme dictates the laser duty cycle. Furthermore, polarization, extinction ratio, and spectral characteristics must be satisfied.
- The effective fight telescope diameter $D_{tx}$ and transmit efficiency $\eta_{tx}$ are determined by the EIRP. Additionally, $D_{tx}$ must provide adequate gain for receiving sufficient beacon, uplink, and ranging laser signal.
- Near-Sun-pointing requirements influence the flight telescope baffling and spatial and spectral filtering design.
- The pointing loss allocation $L_{\text{pointing}}$ dictates the ATP assembly design. The spacecraft platform disturbance power spectral density, as well as, longer term misalignments due to thermal and mechanical drift must be considered. Provision for robust link acquisition and accurate point ahead must also be made.

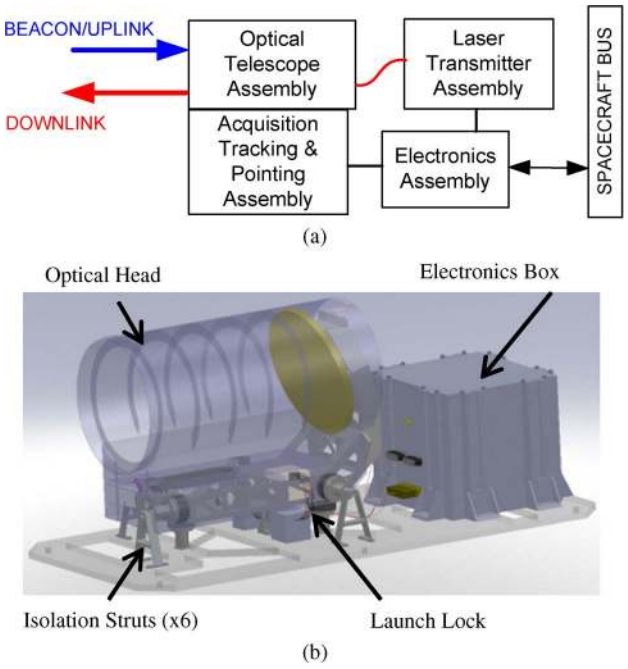


**Fig. 7.** *(a) Generic block diagram for an optical communication terminal. (b) Solid model rendering of a deep-space flight terminal conceptual design [62].*

- The electronics assembly functions are: 1) to ingest user data and process it (Fig. 3) for transmission over the laser beam; 2) to support lasercom terminal command, control, and monitoring including interfacing to spacecraft power, command, and telemetry; 3) to detect and receive uplink and ranging signals.

Following the brief overview of functions of each flight terminal assembly, a short discussion on design implementation considerations for the major flight system assemblies is given below.

*1) Laser Transmitter Assembly:* Choices of lasers suitable for use in deep space are limited by size, mass, power efficiency, ease of modulation at high data-rates, and the ability to extract kW-level peak power pulses with high (1–20 W) average powers. Tolerance to thermal cycling, space radiation, shock, and vibration typically experienced during launch and travel to deep space is required. These diverse requirements limit our choice of lasers to diode-pumped solid-state (bulk crystal or fiber), and specifically Neodymium (Nd), Ytterbium (Yb), or Erbium (Er) doped lasers operating in the 1000–1600-nm wavelength region [55]–[60].

The master-oscillator/power-amplifier (MOPA) laser architecture is favored for deep-space applications. In a MOPA architecture, amplitude stable, single spatial mode, low-power lasers serve as master oscillators that can be directly or externally modulated with encoded data sequences. Subsequent optical amplifier stages provide greater than 30 dB gain thereby increasing the output peak power of the laser assembly to 0.1–1-kW levels while preserving its modulation characteristics. Both 1060- and 1550-nm wavelengths provided by waveguide (fiber or planar crystal) amplifiers are viable as flight laser transmitters. Each provides its own advantages. For example, compared to current 1550-nm lasers, 1060-nm lasers offer superior wall-plug efficiency by nearly a factor of two.

Average output powers on the order of 1–20 W, and peak powers on the order of hundreds of watts to $> 1$ kW are required for typically deep-space links. Destructive nonlinear effects, e.g., stimulated Brillouin scattering (SBS) [61], can limit the peak power achievable. Typical pulse widths are on the order of subnanoseconds to several nanoseconds, and pulse repetition frequencies on the order of from 0.1 to hundreds of megahertz. Self-phase-modulation currently limits the laser pulse widths to approximately 50 ps. Deep-space data rates are not currently limited by the available laser pulse widths. On the other hand, the ability to increase laser pulse width from a few nanoseconds to ten or more nanoseconds will benefit the probability of link acquisition under stressing conditions when background additive noise is high and the signals are faint.

*2) Optical Telescope Assembly:* Implementing the flight telescope with minimum mass and optimal efficiency for the space environment is a major consideration. Use of materials like SiC that provide an excellent combination of relatively low mass and low coefficient of thermal expansion can help with minimizing mass with a thermally stable structure. Use of off-axis telescopes (without a secondary obscuration) in combination with high-quality optical coatings maximizes the efficiency. These terminal architectures can also be designed to point close to the Sun without requiring a separate solar rejection filter [62]. Axisymmetric architectures, on the other hand, usually require a separate solar protection filter at the entrance aperture of the telescope but may be preferred in some cases because they are more compact. Stray light minimization and optical isolation between the received and transmitted laser beams are critical design considerations for the optical telescope assembly. Wavelength diversity of the uplink and downlink is favorably viewed in order to achieve the latter.

The sensors and actuators for ATP, as well as, uplink receivers are integrated into the optical telescope assembly. The sensors and detectors used for receiving the beacon, uplink, and ranging signals must provide adequate sensitivity, field-of-view, resolution, spectral filtering, and bandwidth. More discussions of these components and assemblies are discussed under the ATP assembly.

*3) ATP Assembly:* Downlink beam pointing is the dominant challenge of optical communications from deep space. With optical telescope diameters on the order of

20–50 cm, and transmit wavelengths on the order of 1000–1600 nm, the beam-width transmitted by the spacecraft terminal is on the order of 2–8 $\mu$rad. An efficient link minimizes $L_{\text{pointing}}$ to less than 2 dB. Meeting this allocation necessitates beam pointing to less than 1 $\mu$rad root mean square (rms). At these beam-widths, even from the longest distance to Mars, the typical footprint of the downlink laser beam is a fraction ($\sim$1/10th) of the Earth diameter. Therefore, significant spacecraft platform disturbance and attitude-error suppression will be required to achieve robust pointing.

Ideally, knowledge of the platform disturbance power spectral density sampled over a sufficiently wide frequency band would help in designing control subsystems for rejecting disturbance. Levying requirements on the spacecraft to provide a quiescent disturbance environment is also an option but may limit missions that can take advantage of lasercom. Unfortunately, the knowledge of spacecraft base disturbance power spectral densities (PSDs) is uncertain at best. Enveloping PSDs have been presumed for lasercom system designs with an angular disturbance of 1E-7 rad$^2$/Hz at 0.1 Hz and 1E-15 rad$^2$/Hz at 1 kHz with a 20 dB per decade slope beyond 0.1 Hz. This is shown by the plot labeled "reverse cumulative" in Fig. 8. The integrated rms angular disturbance over the frequency of interest for this PSD is 140 $\mu$rad. The disturbance stems from spacecraft attitude control, reaction wheel vibrations, fuel slosh, solar panel articulation, and sometimes slewing of other instruments onboard the spacecraft.

For RF telecommunication systems that are body mounted to the spacecraft, pointing control to within approximately 1/10 of a degree is implemented [63]. For a body-mounted lasercom systems the spacecraft will control the coarse pointing while the ATP assembly within the flight subsystem will suppress the disturbance jitter to less than 1 $\mu$rad.

On the other hand, for spacecraft where the telecommunication system cannot be body mounted a separate actuator suited to the required field of regard will be required for maintaining line of sight to the receiver. This actuator will serve the coarse pointing function.

As pointed out earlier for deep-space links a weak or dim beacon laser signal from Earth is expected. Strategies to ease acquisition and tracking of such a dim beacon have been identified.

The first strategy is to lower the bandwidth at which the beacon has to be tracked. Two approaches have been studied. The first relies on the use of a local inertial reference source to actively suppress disturbances at required bandwidths, supplemented by a slower bandwidth beacon loop that can correct for bias errors and allow accurate implementation of point-ahead angles [64]. The second approach relies on isolating the optical terminal from the spacecraft disturbance reducing the need for high-bandwidth disturbance suppression [65]. Neither of these has been validated in space. The latter approach with mechanical isolation can be passive, active, or hybrid that combines passive and active. Passive isolators include elastomeric and spring mounts for minimizing mechanical coupling of spacecraft jitter onto the lasercom terminal. Passive isolation alone (low-pass filtering of disturbances) requires very low corner frequencies. Active isolators use electromechanical actuation (e.g., voice coils) for controlling platform isolation. Active isolation alone requires high bandwidths. A hybrid approach combining of passive and active isolation has been found to be optimal for substantial suppression of spacecraft disturbance. Fig. 8 illustrates this where the cumulative pointing error (integration of the disturbance power spectrum) is plotted versus frequency. The cumulative plot approximates a passive isolator with an ideal low-pass filter and the reverse cumulative approximates an active disturbance cancellation mechanism with an ideal high-pass filter.

A second strategy to facilitate the use of a dim beacon is to transmit a modulated beacon which allows subtraction of the background following temporal acquisition of the beacon modulation. Deep-space terminal focal plane array FOVs are slightly larger than the maximum point-ahead angle. For example, if the point-ahead angle is $\pm$400 $\mu$rad a 1-mrad FOV would be appropriate. The space terminal architecture [66] to accommodate this scheme is essential for deep space. High sensitivity of the focal plane array is an added benefit for lowering the beacon power that must be transmitted from the ground. An emerging novel concept [62] combines single photon-counting sensitivity of the focal plane array sensor with subnanosecond time response, so that the same sensor can be used for ATP, receiving uplink and ranging. If suitable devices to implement this concept are developed, in addition to

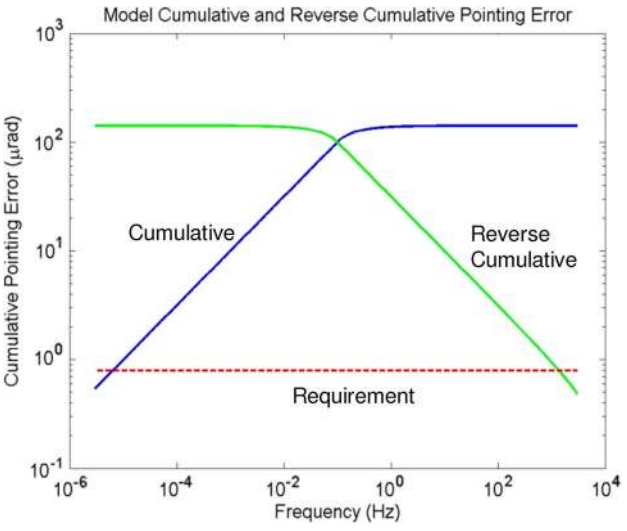


**Fig. 8.** *Cumulative pointing error approximating a passive isolator as a low-pass filter and reverse cumulative approximating active cancellation as an ideal high-pass filter.*

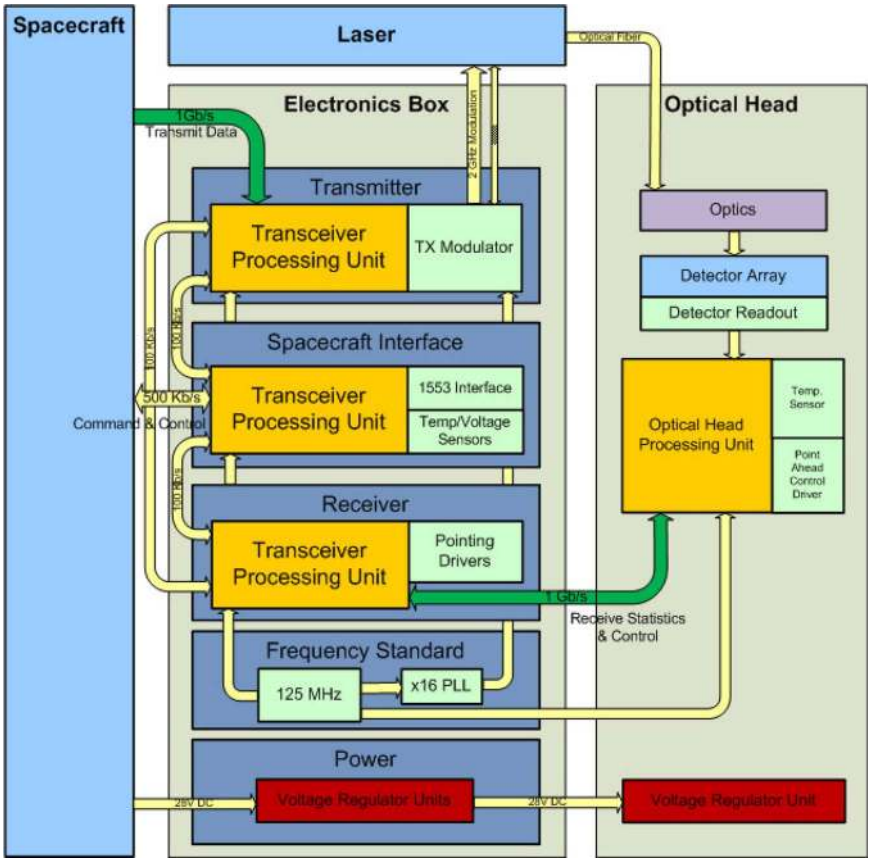


**Fig. 9.** ***Schematic for a JPL-developed electronics architecture with interfaces to the spacecraft and optical telescope assembly shown.***

accomplishing three separate functions with a single sensor, significant resources in terms of mass and power will also be saved by eliminating an uplink receiver assembly.

The use of Earthlight to assist acquisition and tracking from deep space has been considered. This is plagued by several difficulties related first to the incomplete illumination of Earth, for example, when Mars is at closest range the Earth appears like a crescent. Another impediment is the albedo variations due to cloud cover that can introduce significant errors in centroiding of the Earth image [67]. Imaging the Earth using the infrared emission has been studied [31] where the circular disc of Earth is maintained independent of sun illumination geometry. The uniformity of the Earth disc in infrared varies depending on emission characteristics of land, oceans, and cloud cover. For distances to Saturn and beyond, since delivering beacon lasers from the ground may prove extremely difficult, a detailed study for use of the Earth image in the infrared is needed.

*4) Electronics Assembly:* The electronics assembly serves as the "brain" of the laser communication terminal. Implementing the key functions of the electronics assembly involves interfacing to the spacecraft command and data handling (C&DH) and attitude control subsystem (ACS). The interface with the spacecraft C&DH is used for commanding the optical terminal (both commands routed to the spacecraft over the RF back channel and locally generated commands on the spacecraft). The ACS interface provides ephemeris and other position and attitude knowledge required by the lasercom terminals' acquisition and pointing algorithms.

These functions have to be accomplished while minimizing mass, power, and volume burden to the spacecraft. Some additional functions of the electronics assembly are power conditioning and providing a stable clock that meets short- and long-term stability requirements dictated by the communication and ranging requirements.

Fig. 9 schematically illustrates the architecture for a JPL-developed electronics assembly concept for lasercom with interfaces to the spacecraft bus and optical telescope assembly.

### B. Ground Subsystem

The ground subsystem transmits and receives laser signals to/from the spacecraft. As pointed out earlier for near-Earth links both functions can be implemented with 1-m class telescopes. A number of optical ground stations

for servicing these links exist around the world today. They are: 1) NASA's Optical Communication Telescope Laboratory (OCTL) at Table Mountain, CA [68]; 2) NICT (Japan's) Optical Ground Station [12] in Kognei; and 3) ESA's operated Optical Ground Station [19] at Tenerife, Canary Island, Spain. We will focus the present discussion on the deep-space ground subsystem and describe the receiver and transmitter separately.

*1) Ground Receiver:* The primary receiver functions of an optical communication ground subsystem are:

- collecting the laser signal photons transmitted from space and through the atmosphere;
- coupling the collected photons on to a detector after polarization and spatial and spectral filtering;
- detection, synchronization, decoding, and information extraction;
- monitoring itself including the atmosphere and weather.

Fig. 10 shows a generic block diagram for a deep-space ground receiver. Light is collected by the telescope assembly. The large effective aperture diameter needed to satisfy $G_R$ [see (1)] for deep space is of the order of 10–12 m and can be realized with either a single large telescope or an array of smaller telescopes. In Fig. 10, the rectangular gray outline labeled element represents an array element with only one implemented for a single large aperture, whereas $N$ equal diameter elements would provide a $N^{1/2}$ times larger effective diameter. Fig. 11 shows a conceptual view of the alternate implementation schemes of a ground receiver subsystem for deep space [69], [70].

Stray light scattered into the detector has to be minimized by limiting direct solar illumination of the primary mirror. Low bidirectional scatter distribution function (BSDF) of the collecting surfaces, especially those directly exposed to solar or daytime sky exposure, is needed.

The coupling optics in the aft of the telescope assembly in Fig. 10 include: wave-plates for linearizing a circularly polarized laser beam (indicated by Pol in Fig. 10); spatial filters and tip-tilt correction for improving signal-to-noise ratio [71]; and narrow spectral filtering for rejecting additive background light. Important design considerations in selecting the spectral filter are the angle of arrival of the signal, the Doppler shifted laser line width, and the number of temporal modes [22].

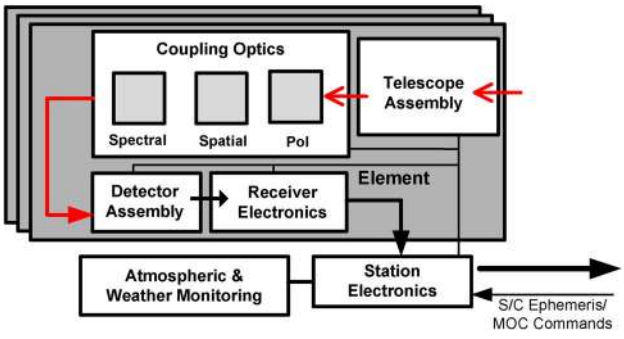


**Fig. 10.** *Generic block diagram for a deep-space ground receiver. The red arrows indicate optical signals while black solid arrows represent flow of downlink data. The dotted black lines indicate electrical/data interfaces.*

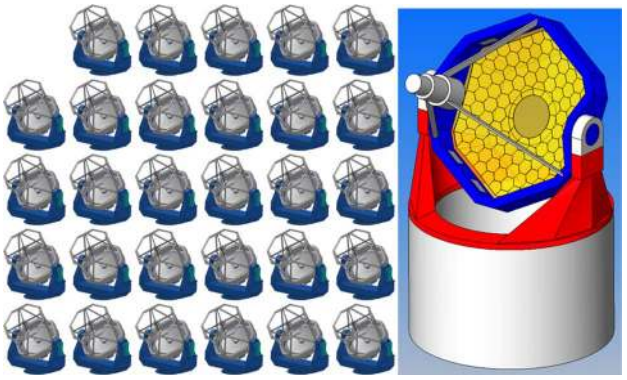

**Fig. 11.** *Comparison of a single 12-m diameter segmented primary telescope conceptual design (right) and an array of 2.2-m diameter telescopes for an equivalent effective diameter. All the telescopes are shown without the domes.*

We briefly discuss some photon-counting detectors for supporting deep-space links.

The intensified photo diode (IPD) is a commercially available product with detection efficiency of 30% at near-infrared downlink wavelengths of 1064 and 1550 nm [43], [72]. The dark noise is 0.1 million counts per second (Mcps) at 1064 nm and 1 Mcps at 1550 nm. The relative large area (1 $mm^2$) detectors have fast rise times and can support minimum slot widths of approximately 500 ps. They are also becoming available as arrays. Modest thermoelectric cooling of these detectors helps to reduce the dark noise. The highest data rates that can be achieved with these detectors is limited by their saturation characteristics, in other words beyond an incident photon-flux rate of ~400 Mcps the counts do not increase. Depending upon the incident additive background photon flux data rates 50–200 Mb/s can be supported; for larger data rates, larger arrays of these detectors will be required.

Niobium nitride (NbN) superconducting nanowire (SN) customized arrays [73] have been demonstrated with detection efficiencies of 50%–78% [74]. For implementation, 50% detection efficiency detector arrays are considered viable. NASA's first optical communication demonstration from lunar distances (see Section V) will be using these detectors. Larger format arrays will be required to cover the FOV of single large-aperture ground-based telescopes and are under development at JPL. The SN arrays operate at cryo-cooled temperatures of 2–3 °K with < 1-Mc/s dark counts. These devices also have excellent detection timing, jitter characteristics, and can support slot

widths of down to 200 ps. The dynamic range or saturation limit of these detectors is also larger. The ability to implement large arrays will also spread the incident photon flux over more pixels thereby further extending the dynamic range.

If an operational deep-space communications system were to be implemented today one would probably rely on IPD detectors, however, in 5–10 years the superconducting nanowire arrays and the cryostats needed to couple them to telescopes are expected to become available.

The deep-space optical receiver technology is based on custom designs demonstrated at Lincoln Laboratory and JPL [33], [75]. They are designed to receive PPM with serially concatenated pulse-position modulation (SCPPM) coding. Some desired characteristics for deep-space receivers are the ability to operate over multiple PPM orders 16 to 256. The ability to extend to higher PPM orders will be useful for farther reaches of deep space. Variable code rates are desired because varying the code rate offers a means of adjusting the link throughput in finer steps. Physical slots of 0.5–8 ns are currently available for deep-space receivers. The lower end is expected to handle 0.2 ns in the near future. The higher end is limited by the laser pulse widths. Logical slot widths by repeating physical slots can be much longer and are needed to support lower data rates of the order of 5–10 kb/s when the background becomes very strong, at Mars farthest ranges, for example.

*2) Deep-Space Ground Transmitter:* The deep-space ground transmitter has been considered as a separate smaller diameter telescope or beam director. The key functions are the capability to deliver a mean irradiance of the order of a few picowatts per square meter ($pW/m^2$) to illuminate the aperture of a flight terminal on a spacecraft at deep-space distances.

The lasers transmitted from the ground can serve multiple functions, namely: 1) a beacon or pointing reference; 2) a carrier for uplink data; and 3) for transmitting laser pulses to facilitate ranging [76].

Even for a beacon-only function, a low-rate modulation is applied to help acquisition and background subtraction at the flight terminal receiver. The low-rate modulation can support low-rate commands of a few bits per second. Since scheduling of deep-space-to-ground optical links will always be subject to vagaries of the atmospheric conditions, real-time commands transmitted from the ground can be very useful in operating the link optimally. Thus, the low-rate commands are a useful feature.

For higher uplink data rates, the demands on the repetition rates of the multi-kW ground transmitter laser system increases as does the requirements on the receiver on the flight terminal. Ranging does not require any additional power but the timing of transmitted and received laser pulses must be known with higher certainty ($< 1$ ns).

Since the ground transmitted lasers propagate through the atmosphere without adaptive optics corrections, multibeaming [28], [77] is used to mitigate scintillation effects. Multibeaming is accomplished by transmitting multiple mutually incoherent, coaligned beamlets. These beamlets can be transmitted through subapertures of a single telescope. The beam centers are separated by distances greater than $r_0$. Two advantages of this strategy are: 1) the multi-kW laser power can be divided among several laser beams while providing redundancy and 2) the averaging of the uncorrelated irradiance fluctuations due to atmospheric scintillation reduces the overall irradiance fluctuations at the aperture of the flight terminal. Thus, the fades are reduced to a level that allows the beacon to be used as a pointing reference.

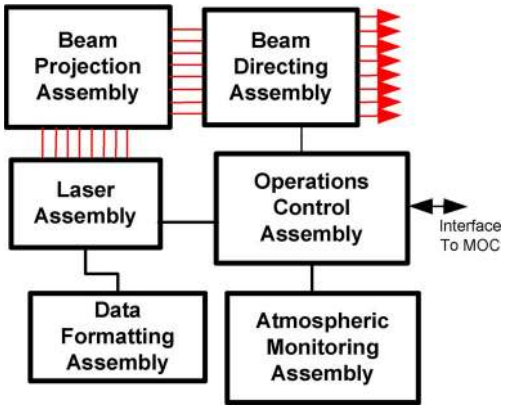


**Fig. 12.** ***Generic block diagram for a deep-space ground transmitting station. The red arrow lines indicate the optical path. The ground transmitting station interfaces to a mission operations center (MOC).***

Fig. 12 shows a generic block diagram for a ground transmitter station for deep space.

Ground transmitting stations must also conform to the entire regulatory agency restrictions on transmitting laser beams into free space. A safety system to ensure this is an integral part of the operations control assembly and is shown in Fig. 12. Interruptions in beacon transmission are expected in the course of operations and a strategy for accommodating these interruptions is required. The safety functions are assumed to be included in the operations control assembly block in Fig. 12.

## V. FUTURE PERSPECTIVES

Future near-Earth optical communication services are on the threshold of becoming operational in the wake of the successful demonstrations listed in Table 1.

The near-Earth user community predominantly Earth observing science spacecraft will be flying instruments that generate huge volumes of data. An example is mission concepts such as Deformation, Ecosystem Structure, and Dynamics of Ice (DesDynI) [78], where the Earth will be simultaneously mapped with synthetic aperture radar (SAR) and light detection and ranging (LIDAR) to provide

high-resolution maps of the surface contours. Other missions that utilize SAR and hyperspectral imaging cameras will also require high rates to get the data back to scientists. This class of missions will be challenging even for the capabilities of laser communications that can support 10-Gb/s instantaneous data rates. The contact time with ground stations for a typical LEO spacecraft is limited and given weather uncertainties will require a global network with interconnectivity on the ground.

Utilizing space-to-space near-Earth links for LEO-to-GEO on the other hand will free the service from the contact time limitations and weather. The European Space Agency is planning a new Data Relay Satellite (EDRS) system to be deployed in 2013 that will provide 2.8 Gb/s over LEO-to-GEO satellite distances of 45 000 km [79].

Similarly, the Japanese Space Agency (JAXA) is also planning a LEO-to-GEO 2.5-Gb/s optical service where the data rate is restricted by the Ka-band link capacity to relay data back to Earth [80].

Both of the above systems are based on coherent intersatellite links similar to the LEO-to-LEO demonstration in Table 1 [14].

Lunar exploration architecture studies have considered the use of optical links from a lunar orbiting spacecraft to Earth ground stations. Extending this service in the future to space-to-space links from Moon-orbiting to Earth-orbiting spacecraft will no doubt follow.

NASA is currently developing the Lunar Laser Communication Demonstration (LLCD) [81] where the Lunar Atmospheric Dust Environment Exploration (LADEE) spacecraft will host an optical terminal being developed by MIT Lincoln Laboratory (MIT-LL) and NASA-Goddard. The demonstration is currently planned for 2013 with downlink data rates of 622 Mb/s and uplink of 20 Mb/s. With this demonstration NASA will validate beyond Earth orbit high-rate optical capability for the first time.

Technology development since the MLCD project has spurred advances in several areas that further accentuate lasercom's promise of providing a comprehensive optical communication service extending to deep-space distances. Rendering such a service operational is feasible by 2025 provided key risk retiring deep-space demonstrations can be initiated by the end of this decade. Having this added capability will enhance the communication and navigation "tool box" for future space missions.

Taking advantage of NASA-sponsored technology developed following MLCD termination, JPL was recently tasked with the concept design of flight and ground terminals resulting in appreciably higher data rate, and lower mass and power than MLCD. This project is called deep-space optical terminals (DOT) [29]. The DOT concept study targeted a 0.25-Gb/s downlink from 0.42 AU (near-Mars distance), while closing the link at 2.7 AU (Mars farthest distance) where the SEP angle was 5°. Furthermore, a requirement was to demonstrate this capability with resources similar to what was used by the Ka-band telecommunication system on MRO (37 kg and 100 W). A 22-cm diameter light-weighted flight telescope with a 4-W average power laser at 1550 nm satisfied this requirement. An 11.8-m effective diameter astronomical telescope was required to demonstrate the maximum data rate while operating under nighttime conditions on Earth. A new 2.2-m diameter telescope conceptual design for pointing to within 5° of the Sun would be used to acquire the link under nominal atmospheric conditions encountered on mountaintop locations of the southwestern United States.

The DOT flight terminal architecture can potentially be matured into designs that could be utilized for optical link demonstrations, such as, Lagrange astrophysics missions, near-Earth object (NEO) missions or Mars missions. Other opportunities may be missions to Jupiter and Venus. For a Jupiter mission, long durations are available during the cruise phase when a link demonstration could be completed. Limited mass and power margins typical for many of these missions make accommodation challenging and demand aggressive resource utilization in optical terminal design.

European studies and activities are also underway in order to migrate optical technologies to servicing deep-space optical links [82], [83].

Access links for the Moon and Mars are also attractive augmentations for future optical service on deep-space missions. In combination with an augmented Mars-to-Earth (trunk-line) optical data-rate capability, for example, imagery from the surface could be streamed up to an orbiter for relay back to Earth in near real time. When Mars is close to Earth the light time of 3–4 min could allow interactive control of Mars surface probes, with this capability.

To benefit from the strength of optical communication technology and not be stymied by its pitfalls future space missions should perform studies to realistically evaluate their telecommunication needs while taking into account the fact that missions will not rely solely on optical communication but some combination of optical and RF communication. Identifying the lowest burden combination of such a telecommunications package will help missions to utilize the optical communication high-rate capability when it is available and the low-rate but highly reliable RF links for telemetry and other critical mission operations.

Protocols and standardization are other aspects of any new telecommunications band. The lasercom physical layer can in principle accommodate most telecommunication protocols. Implementation details, such as transmit/receive wavelengths, direct or coherent reception, modulation, and coding, will be the subject of future international committees such as the Consultative Committee for Space Data Systems (CCSDS).

## VI. SUMMARY

In this paper, we described a high level, broad overview of the state of optical communications technology, both

current and future perspectives. The special aspects of using optical communications for servicing deep space have been emphasized with comparisons to near Earth when applicable. Optical communications (lasercom) from deep space is a new frontier awaiting initial technology demonstrations, which will result in augmented missions for space science and exploration. ■

## APPENDIX
## ERROR PROBABILITIES OF VARIOUS MODULATION SCHEMES

For the Poisson channel in the presence of background radiation, characterized by the average number of background photons $K_b$, the corresponding pdfs are given by

$$f_{Y|X}(k|0) = K_b^k e^{-K_b}/k! \text{ and}$$
$$f_{Y|X}(k|1) = (K_s + K_b)^k e^{-(K_s+K_b)}/k!$$

The LLR for OOK becomes $L(k) = K_s - k\log(1 + K_s/K_b)$ and corresponding ML detector is in fact the threshold detector

$$\hat{x} = \begin{cases} 1, & y > y_{\text{tsh}} \\ 0, & y \le y_{\text{tsh}} \end{cases}; \qquad y_{\text{tsh}} = K_s/\log\left(1 + \frac{K_s}{K_b}\right). \quad \text{(A1)}$$

The BER can be determined by

$$P_b = \frac{1}{2} - \frac{1}{2}\sum_{l=0}^{\lfloor y_{\text{tsh}} \rfloor}[f(k|0) - f(k|1)] \quad \text{(A2)}$$

which in the absence of background radiation becomes simply

$$P_b = \frac{1}{2}e^{-K_s}. \quad \text{(A3)}$$

For direct detection of PPM, when a continuous-output channel model is observed, the symbol error probability is the symbol error probability of an ML detector for $M$-ary orthogonal signaling

$$P_s = 1 - \int_{-\infty}^{\infty} f_{Y|X}(y|1)\left[\int_{-\infty}^{y} f_{Y|X}(y'|0)dy'\right]^{M-1} dy \quad \text{(A4)}$$

where the observations in $M-1$ nonsignaling slots are assumed to be independent. When the detector outputs take on discrete values, the corresponding symbol error probability is

$$P_s = 1 - \frac{1}{M}\sum_{k=0}^{\infty} l(k)\left[F_{Y|X}(k|0)^M - F_{Y|X}(k-1|0)^M\right] \quad \text{(A5)}$$

where $l(k)$ is likelihood ratio and $F_{Y|X}(k|i)$ is the cumulative distribution function (CDF). For Poisson channel, in the presence of background photons $K_b$, the symbol error probability expression (A5) becomes

$$P_s = 1 - \sum_{k=0}^{\infty}\left(1 + \frac{K_s}{K_b}\right)^k \frac{e^{-K_s}}{M}\left[F_{Y|X}(k|0)^M - F_{Y|X}(k-1|0)^M\right] \quad \text{(A6)}$$

where CDF is determined by

$$F_{Y|X}(k|0) = \sum_{m=0}^{k} K_b^m e^{-K_b}/m!$$

In the absence of background radiation, the symbol error probability expression becomes simply

$$P_s = (M-1)e^{-K_s}/M \quad \text{(A7)}$$

and corresponding $P_b$ is the same as that for OOK.

## REFERENCES


[1] J. W. Layland and L. L. Rauch. (1997, Aug. 15). The evolution of technology in the deep space network: A history of the advanced systems program. The Telecommunications and Data Acquisition Progress Rep. 42-130. [Online]. Available: http://tmo.jpl.nasa.gov/progress_report/42-130/title.htm

[2] B. Geldzahler and L. Deutsch. (2009, Sep. 1). Future plans for the deep space network (DSN). White Paper, Planetary Decadal Survey 2013-2022. [Online]. Available: http://www.lpi.usra.edu/decadal/sbag/topical_wp/geldzahler.pdf

[3] R. J. Cesarone, D. S. Abrahams, S. Shambayati, and J. Rush, "Deep space communications, visions trends and prospects," in *Proc. Int. Conf. Space Opt. Syst. Appl.*, Santa Monica, CA, May 11–13, 2011, pp. 412–425.

[4] J. S. Schier, J. J. Rush, W. Dan Williams, and P. Vrotsos, "Space communication architecture supporting exploration and science: Plans and Studies for 2010–2030," in *Proc. 1st Space Exploration Conf., Continuing the Voyage of Discovery*, Orlando, FL, Jan. 30–Feb. 1, 2005, vol. 1, pp. 2005–2517.

[5] W. D. Williams, M. Collins, D. M. Boroson, J. Lesh, A. Biswas, R. Orr, L. Schuchman, and O. S. Sands, "RF and optical communications: A comparison of high data rate returns from deep space in the 2020 timeframe," presented at the 12th Ka and Broad Band Commun. Conf., Naples, Italy, Sep. 27–29, 2006, Paper K00083.

[6] H. Hemmati, Ed., *Deep Space Optical Communications*. New York: Wiley, 2006.

[7] B. G. Boone, J. R. Bruzzi, and B. E, "Optical communications development for spacecraft applications," *John Hopkins APL Tech. Dig.*, vol. 25, no. 4, pp. 306–315, 2004.

[8] K. E. Wilson and J. R. Lesh, "Overview of the ground-to-orbit lasercom demonstration," *Proc. SPIE—Free-Space Laser Commun. Technol. IX*, vol. 2990, pp. 1–9, Jan. 1997.

[9] J. Keller, "Optical links are key to next-generation military communications satellites," *Military Aerosp. Electron.*, vol. 15, no. 4, Apr. 1, 2004. [Online]. Available: http://mae.pennnet.com/articles/article_display.cfm?article_id=202216

[10] T. Tolkeer-Nielsen and G. Oppenhauser, "In-orbit test results of an operational intersatellite link between ARTEMIS and SPOT4, silex," *Proc. SPIE—Free-Space Laser Commun. Technol. IX*, vol. 3615, pp. 31–42, Apr. 1999.

[11] H. Hemmati, Ed., *Near-Earth Laser Communications*. Boca Raton, FL: CRC Press, 2009, p. 24.

[12] M. Toyoshima *et al.*, "Results from phase-1, phase-2 and phase-3 kirari optical communication demonstration experiments with the NICT optical ground station (KODEN)," in *Proc. 25th AIAA Int. Commun. Satellite Syst. Conf.*, 2007, AIAA 2007-3228.

[13] L. Vaillon, G. Planche, V. Chorvilli, and L. Le Hors, "Optical communications between an aircraft and a GEO relay satellite: Design & flight results of the LOLA demonstrator," in *Proc. 7th Int. Conf. Space Opt.*, 2008.

[14] B. Smutny *et al.*, "In-orbit verification of optical inter-satellite communication links based on homodyne BPSK," *Proc. SPIE—Free-Space Laser Commun. Technol. XX*, vol. 6877, pp. 687702-1–687702-6, 2008.

[15] K. E. Wilson and J. R. Lesh, "An overview of the Galileo Optical Experiment (GOPEX), JPL TDA Progr. Rep. 421-114, Aug. 15, 1993.

[16] D. E. Smith, M. T. Zuber, X. Sun, G. A. Neumann, J. F. Cavanaugh, J. F. McGarry, and T. W. Zagwodzki, "Two-way laser link over interplanetary distance," *Science*, vol. 311, p. 53, 2006.

[17] A. Biswas, D. Boroson, and B. Edwards, "Mars laser communications demonstration: What it would have been," *Proc. SPIE—Free-Space Laser Commun. Technol. XVII*, vol. 6105, pp. 610502-1–610502-12, 2006.

[18] S. F. Franklin *et al.*, "The 2009 Mars telecom orbiter mission," in *Proc. IEEE Aerosp. Conf.*, Mar. 2004, vol. 1, pp. 437–4566–113.

[19] R. H. Clichy, Z. Sonic, and B. Furch, "Design of an optical ground station for in-orbit check-out of free-space laser communication payloads," *Proc. SPIE—Free-Space Laser Commun. Technol. VII*, vol. 2381, pp. 26–37, 1995.

[20] M. Reyes *et al.*, "Preliminary results of the in-orbit test of ARTEMIS with optical ground station," *Proc. SPIE—Free-Space Laser Commun. Technol. XIV*, vol. 4635, pp. 38–49, 2002.

[21] K. E. Wilson *et al.*, "Preliminary results of the OCTL to OICETS optical experiment (OTOOLE)," *Proc. SPIE—Free-Space Laser Commun. Technol. XXII*, vol. 7587, pp. 758703-1–758703-13, 2010.

[22] R. M. Gagliardi and S. Karp, *Optical Communications*, 2nd ed. New York: Wiley, 1995, pp. 92–99.

[23] R. Fields, D. Kozlowski, H. Yura, R. Wong, J. Wicker, C. Lunde, M. Gregory, B. Wandernoth, and F. Heine, "5.625 Gbps bidirectional laser communications measurements between the NFIRE satellite and an optical ground station," in *Proc. Int. Conf. Space Opt. Syst. Appl.*, Santa Monica, CA, May 11–13, 2011, pp. 44–53.

[24] NASA. [Online]. Available: http://map.gsfc.nasa.gov/mission/observatory_l2.html

[25] D. M. Boroson, A. Biswas, and B. L. Edwards, "MLCD: Overview of NASA's Mars laser communications demonstration system," *Proc. SPIE—Free-Space Laser Commun. Technol. XVI*, vol. 5338, pp. 16–28, 2004.

[26] L. C. Andrews and R. L. Phillips, *Laser Beam Propagation Through Random Media*. Bellingham, WA: SPIE Optical Press, 1998, ch. 9, p. 253.

[27] A. Biswas, F. Khatri, and D. Boroson, "Near-sun free-space optical communications from space," in *Proc. IEEE Aerosp. Conf.*, Big Sky, MT, 2006.

[28] A. Biswas, M. W. Wright, J. Kovalik, and S. Piazzolla, "Uplink beacon laser for Mars Laser Communication Demonstration (MLCD)," *Proc. SPIE—Free-Space Laser Commun. Technol. XVII*, vol. 5712, pp. 93–100, 2005.

[29] A. Biswas, H. Hemmati, S. Piazzolla, B. Moision, K. Birnbaum, and K. Quirk. (2010, Nov. 15). Deep space optical terminals (DOT) system engineering. Interplanetary Netw. Progr. Rep. 42-183. [Online]. Available: http://tmo.jpl.nasa.gov/progress_report/42-183/183A.pdf

[30] C. Chen, J. W. Alexander, H. Hemmati, S. Monacos, T. Yan, J. R. Lesh, and S. Zingales, "System requirements for a deep space optical transceiver," *Proc. SPIE—Free-Space Laser Commun. Technol. XI*, vol. 3615, pp. 142–152, 1999.

[31] A. Biswas, S. Piazzolla, G. Peterson, G. G. Ortiz, and H. Hemmati. (2006, Nov. 15). The long-wave infrared Earth image as a pointing reference for deep space optical communications. Interplanetary Netw. Progr. Rep. 42-167. [Online]. Available: http://tmo.jpl.nasa.gov/progress_report/42-167/title.htm

[32] J. A. Mendenhall, L. M. Candell, P. I. Hopman, G. Zogbi, D. M. Boroson, D. O. Caplan, C. J. Digenis, D. R. Hearn, and R.C. Shoup, "Design of an optical photon counting array receiver system for deep space communications," *Proc. IEEE*, vol. 95, *Special Issue Technical Advances in Deep Space Communications and Tracking: Part I*, no. 10, pp. 2059–2069, Oct. 2007.

[33] A. Biswas, B. Moision, W. T. Roberts, W. H. Farr, A. Gray, K. Quirk, J. Hamkins, M. K. Cheng, J. Gin, M. Nakashima, G. G. Ortiz, S. Piazzolla, C. C. Liebe, and D. L. Losh, "Palomar Receive Terminal (PRT) for the Mars Laser Communication Demonstration (MLCD) project," *Proc. IEEE*, vol. 95, *Special Issue Technical Advances in Deep Space Communications and Tracking: Part I*, no. 10, pp. 2045–2058, 2007.

[34] M. Britcliffe, D. Hoppe, W. Roberts, and N. Page, "A ten-meter ground station telescope for deep space optical communications: A preliminary design," Interplanetary Netw. Progr. Rep. 42-147, Nov. 15, 2001.

[35] D. O. Caplan, "Laser communication transmitter and receiver design," *J. Opt. Fiber Commun. Rep.*, vol. 4, pp. 225–362, 2007.

[36] G. S. Wojcik *et al.*, "Deep space to ground laser communications in a cloudy world," *Proc. SPIE—Free-Space Laser Commun. V*, vol. 5892, pp. 589203-1–589203-11, 2005.

[37] W. J. Hurd, B. E. MacNeal, G. G. Ortiz, R. V. Moe, J. Z. Walker, M. L. Dennis, E. S. Cheng, D. A. Fairbrother, B. Eegholm, and K. J. Kasunic, "Exo-atmospheric telescopes for deep space optical communications," in *Proc. IEEE Aerosp. Conf.*, Big Sky, MT, Mar. 2006.

[38] C. D. Edwards, Jr. and R. DePaula, "Key telecommunications technologies for increasing data return for future Mars exploration," *Acta Astronautica*, vol. 61, pp. 131–138, 2007.

[39] A. Biswas, J. Kovalik, M. W. Regehr, and M. Wright, "Emulating and optical planetary access link with an aircraft, and Low complexity transceivers and autonomous concept of operations for optical planetary access links," in *Proc. Free-Space Laser Commun. Technol. XXII*, 2010, vol. 7587, 75870B, 2010.

[40] B. J. Klein and J. J. Degnan, "Optical antenna gain. 1: Transmitting antennas," *Appl. Opt.*, vol. 13, pp. 2134–2141, Sep. 1974.

[41] V. Mahajan, *Aberration Theory Made Simple*, vol. TT6. Bellingham, WA: SPIE, pp. 138–142.

[42] K. J. Quirk, J. Gin, and M. Srinivasan, "Optical PPM synchronization for photon counting receivers," in *Proc. IEEE Military Commun. Conf.*, 2008, DOI: 10.1109/MILCOM.2008.4753054.

[43] K. Birnbaum, W. Farr, J. Gin, B. Moision, K. Quirk, and M. Wright, "Demonstration of a high-efficiency free-space optical communications link," *Proc. SPIE—Free-Space Laser Commun. Technol. XXII*, vol. 7199, pp. 71990A-1–71990A-12, 2009.

[44] S. Piazzolla, *Deep-Space Optical Communications*, H. Hemmati, Ed. New York: Wiley, 2006, pp. 237–270.

[45] H. Hemmati, A. Biswas, and D. Boroson, "Prospects for improvement of interplanetary laser communication data rates by 30 dB," *Proc. IEEE*, vol. 95, *Special Issue: Technical Advances in Deep Space Communications and Tracking: Part I*, no. 10, pp. 2082–2092, Oct. 2007.

[46] S. J. Dolinar, J. Hamkins, B. E. Moision, and V. A. Vilnrotter, *Deep-Space Optical Communications*, H. Hemmati, Ed. New York: Wiley, 2006, pp. 215–289.

[47] G. M. Lee and G. W. Schroeder, "Optical PPM with multiple positions per pulse width," *IEEE Trans. Commun.*, vol. COM-25, no. 3, pp. 360–364, Mar. 1977.

[48] D. Zwillinger, "Differential PPM has a higher throughput than PPM for the band-limited and average-power-limited optical channel," *IEEE Trans. Inf. Theory*, vol. IT-34, no. 5, pp. 1269–1273, Sep. 1988.

[49] R. J. McIntyre, "The distribution of gains in uniformly multiplying avalanche photodiodes: Theory," *IEEE Trans. Electron. Devices*, vol. ED-19, no. 6, pp. 703–713, Jun. 1972.

[50] P. P. Webb, R. J. McIntyre, and J. Conradi, "Properties of avalanche photodiodes," *RCA Rev.*, vol. 35, pp. 234–278, Jun. 1974.

[51] B. Moision and J. Hamkins. (2000, Aug. 15). Deep space optical communications downlink budget: Modulation and coding. Jet Propulsion Laboratory, Pasadena, CA, Interplanetary Netw. Progr. Rep. 42-154, Apr.–Jun. 2003, pp. 1–28. [Online]. Available: http://ipnpr.jpl.nasa.gov/progress_report/42-154/154K.pdf

[52] B. Moision and J. Hamkins. (2005, May 15). Coded modulation for the deep space optical channel: Serially concatenated pulse-position modulation. Jet Propulsion Laboratory, Pasadena, CA, Interplanetary Netw. Progr. Rep. 42-161, pp. 1–25. [Online]. Available: http://ipnpr.jpl.nasa.gov/progress_report/42-161/161T.pdf

[53] M. F. Barsoum, B. Moision, M. Fitz, D. Divsalar, and J. Hamkins, "Iterative coded pulse-position-modulation for deep space optical communications," in *Proc. Inf. Theory Workshop*, Lake Tahoe, CA, Sep. 2–6, 2007, pp. 66–71.

[54] I. B. Djordjevic, W. Ryan, and B. Vasic, *Coding for Optical Channels*. New York: Springer-Verlag, 2010.

[55] H. Zellner, U. Williamowski, A. Tunnerman, H. Welling, S. Unger, V. Reichel, H.-R. Muller, and J. Kirchof, "High-power CW neodymium-doped fiber laser operating at 9.2 W with high beam quality," *Opt. Lett.*, vol. 20, pp. 578–580, 1995.

[56] K. Du, N. Wu, J. Xu, J. Giesekus, P. Loosen, and R. Poprawe, "Partially end-pumped Nd: YAG slab laser with a hybrid resonator," *Opt. Lett.*, vol. 23, pp. 370–372, 1998.

[57] Y. Jeong, J. K. Sahu, D. N. Payne, and J. Nilsson, "Ytterbium-doped large core fiber laser with 1.36 kW continuous-wave output power," *Opt. Exp.*, vol. 12, pp. 6088–6092, 2004.

[58] T. S. Rutherford, W. M. Tulloch, S. Sinha, and R. L. Byer, "Yb:YAG and Nd:YAG edge-pumped slab lasers," *Opt. Lett.*, vol. 26, pp. 986–988, 2001.

[59] J. Dong, W. H. Loh, J. E. Caplan, and J. D. Minelly, "Efficient single-frequency fiber lasers with novel photosensitive Er/Yb optical fibers," *Opt. Lett.*, vol. 22, pp. 694–696, 1997.

[60] G. Huber, E. W. Duczynski, and K. Peterman, "Laser pumping of Ho-, Tm-, Er-doped garnet laser at room temperature," *IEEE J. Quantum Electron.*, vol. QE-24, no. 6, pp. 920–923, Jun. 1988.

[61] N. W. Spellmeyer, D. O. Caplan, B. S. Robinson, D. Sandberg, M. L. Stevens, M. M. Willis, D. V. Gapontsev, N. S. Platonov, and A. Yusim, "A high-eficiency Ytterbium-doped fiber amplifier designed for interplanetary laser communication," presented at the Opt. Fiber Commun. Conf., Anaheim, CA, Mar. 25, 2007, paper OMF2.

[62] W. H. Farr, M. W. Regehr, M. Wright, D. Sheldon, A. Sahasrabudhe, J. Gin, and D. Nguyen, "Overview and trades for the DOT flight laser transceiver," Interplanetary Netw. (IPN) Progr. Rep. 42-184.

[63] S. W. Lee and E. D. Skulsky, "Mars reconnaissance orbiter design approach for high resolution surface imaging," in *Proc. 26th Annu. Amer. Astronaut. Soc. Guid. Control Conf.*, Feb. 2003, pp. 03–067.

[64] J. W. Burnside, D. V. Murphy, F. K. Knight, and F. I. Khatri, "A hybrid stabilization approach for deep space optical communications terminals," *Proc. IEEE*, vol. 95, *Special Issue Technical Advances in Deep Space Communications and Tracking: Part I*, no. 10, pp. 2070–2081, Oct. 2007.

[65] C.-C. Chen, H. Hemmati, A. Biswas, G. Ortiz, and W. Farr, "Simplified lasercom system architecture using a disturbance-free platform," *Proc. SPIE*, vol. 6105, pp. 610505–610505-6, 2006.

[66] C. C. Chen and J. R. Lesh, "Overview of the optical communications demonstrator," *Proc. SPIE*, vol. 2123, pp. 85–94, 1994.

[67] C.-C. Chen. Effect of Earth Albedo variation on the performance of a spatial acquisition subsystem aboard a planetary spacecraft. Interplanetary Netw. Progr. Rep. 42-95, Jul.–Sep. 1988. [Online]. Available: http://tmo.jpl.nasa.gov/progress_report/42-167/title.htm

[68] K. E. Wilson, N. Page, J. Wu, and M. Srinivasan. The JPL Optical Communications Telescope Laboratory test bed for the Future Optical Deep Space Network. Jet Propulsion Laboratory, Pasadena, CA, Interplanetary Netw. Progr. Rep. 42153, Jan.–Mar. 2003. [Online]. Available: http://ipnpr.jpl.nasa.gov/progress-report/

[69] K. Birnbaum. (2010, Aug.). DOT ground laser receiver: Overview and major trades. Interplanetary Netw. Progr. Rep. 42-182. [Online]. Available: http://tmo.jpl.nasa.gov/progress_report/42-182/title.htm

[70] T. Sebring, *Private Communication*, Jul. 2010.

[71] A. Biswas *et al.*, "Approach for acquiring and tracking downlink from Mars using the hale telescope," *Proc. SPIE*, vol. 5712, pp. 60–71, 2005.

[72] R. A. La Rue, K. A. Costello, C. A. Davis, J. P. Edgecumbe, and V. W. Aebi, "Photon counting II-V hybrid photomultipliers using transmission mode photocathodes," *IEEE Trans. Electron Devices*, vol. 44, no. 4, pp. 672–678, Apr. 1997.

[73] J. A. Stern and W. H. Farr, "Fabrication and characterization of superconducting NbN nanowire single photon detectors," *IEEE Trans. Appl. Supercond.*, vol. 17, no. 2, pp. 306–309, Jun. 2007.

[74] K. M. Rosfjord, J. K. W. Yang, E. A. Dauler, A. J. Kerman, V. Anant, B. M. Voronov, G. N. Gol'tsman, and K. K. Berggren, "Nanowire single-photon detector with an integrated optical cavity and anti-reflection coating," *Opt. Exp.*, vol. 14, no. 2, pp. 527–534, 2006.

[75] K. J. Quirk and J. W. Gin, "Optical PPM combining loss for photon counting receivers," in *Proc. IEEE Military Commun. Conf.*, 2006, DOI: 10.1109/MILCOM.2006.301986.

[76] K. M. Birnbaum, Y. Chen, and H. Hemmati, "Precision optical ranging by paired one-way time of flight," *Proc. SPIE—Free-Space Laser Commun. Technol. XXII*, vol. 7587, pp. 75870A-1–75870A-8, 2010.

[77] W. T. Roberts and M. W. Wright. (2010, Nov.). Deep space optical terminals (DOT) ground laser transmitter (GLT) trades and conceptual point design. Interplanetary Netw. Progr. Rep. 42-183. [Online]. Available: http://tmo.jpl.nasa.gov/progress_report/42-183/183C.pdf

[78] W. T. K. Johnson, P. A. Rosen, S. Hensley, and A. Freeman, "Radar designs for the DESDynI mission," in *Proc. IEEE Aerosp. Conf.*, Mar. 2009, DOI: 10.1109/RADAR.2009.4977119.

[79] Z. Sodnik, H. Lutz, B. Furch, and R. Meyer, "Optical satellite communications in Europe," *Proc. SPIE*, vol. 7587, pp. 758705-1–758705-9, 2010.

[80] S. Yamakaw, T. Hanada, H. Kohata, and Y. Fujiwara, "JAXA's efforts toward next generation space data-relay satellite using optical inter-orbit communication technology," *Proc. SPIE*, vol. 7587, pp. 758705-1–758705-9, 2010.

[81] B. S. Robinson, D. M. Boroson, D. A. Burianek, and D. V. Murphy, "Overview of the lunar laser communication demonstration *Proc. SPIE—Free-Space Laser Commun. Technol. XXII*, vol. 7923, pp. 792302-1–792302-4, 2011.

[82] F. Castellini, A. Simonetto, R. Martini, and M. Lavagna, "A Mars communication constellation for human exploration and network science," *Adv. Space Res.*, vol. 45, pp. 183–199, 2005.

[83] T. Dreischer, F. Arnold, K. Kudielka, Y. Tissot, and T. Weigel, "Lasercom for interplanetary missions—Recent European activities, future possibilities and synergy aspects," *Proc. SPIE*, vol. 7587, pp. 758704-1–758704-12, 2010.

## ABOUT THE AUTHORS

**Hamid Hemmati** (Senior Member, IEEE) received the M.S. degree from USC and the Ph.D. degree from CSU, both in physics.

He is currently with the Jet Propulsion Laboratory (JPL), California Institute of Technology, Pasadena, where he is a Principal member of staff and the Supervisor of the Optical Communications Group. Prior to joining JPL in 1986, he was a researcher at NASA's Goddard Space Flight Center and at NIST, Boulder, CO. He teaches lasercom at the University of California Los Angeles (UCLA). He has published over 160 journal and conference papers and holds seven patents. He is the editor and author of two books: *Deep Space Optical Communications* (NJ: Wiley Interscience, 2006) and *Near-Earth Laser Communications* (Boca Raton, FL: CRC Press, 2009). His current research interests are in developing lasercom technologies and low mass/power/size flight terminals for both interplanetary and satellite communications. His research activities include: electro-optical systems engineering, solid-state lasers (particularly pulsed fiber lasers), flight qualification of optical and electro-optical systems and components; low-cost multimeter diameter optical ground receiver telescopes; active and adaptive optics; and laser beam acquisition, tracking, and pointing.

Dr. Hemmati is a Fellow of the SPIE—The International Society for Optics and Photonics, and 2011 recipient of NASA's Exceptional Service Medal.

**Abhijit Biswas** received the Ph.D. degree in molecular science from Southern Illinois University at Carbondale in 1986.

Currently, he is a Senior Telecommunications Engineer with the Optical Communications Group, Jet Propulsion Laboratory (JPL), California Institute of Technology, Pasadena. He has been involved in system engineering and end-to-end field demonstrations related to free-space optical communications for the past 14 years. Prior to this he worked in the areas of laser light scattering and laser spectroscopy (Raman and fluorescence) spectroscopy as a diagnostic for containerless processing. He also was a research associate with the Physics Department, New Mexico State University, where his research was in the area of optical levitation and nonlinear optical interactions between high-energy lasers and aerosols. He also worked in the area of photoacoustic microscopy as a part of his Ph.D. dissertation. He has published over 85 conference and journal papers.

**Ivan B. Djordjevic** (Senior Member, IEEE) received the Dipl.Ing., M.Sc., and Ph.D. degrees from the University of Nis, Serbia, in 1994, 1997, and 1999, respectively, all in electrical engineering.

He is currently an Assistant Professor in the Department of Electrical and Computer Engineering, University of Arizona, Tucson, with a joint appointment in the College of Optical Sciences. Prior to this appointment in August 2006, he was with University of Arizona (as a Research Assistant Professor); University of the West of England, Bristol, U.K.; University of Bristol, Bristol, U.K.; Tyco Telecommunications, Eatontown, NJ; and the National Technical University of Athens, Athens, Greece. His current research interests include optical networks, error control coding, constrained coding, coded modulation, turbo equalization, OFDM applications, and quantum error correction. He presently directs the Optical Communications Systems Laboratory (OCSL), Department of Electrical and Computer Engineering, University of Arizona. He is an author, together with Dr. W. Shieh, of the book *OFDM for Optical Communications* (New York: Elsevier, Oct. 2009). He is also an author, together with Prof. Ryan and Prof. Vasic, of the book *Coding for Optical Channels* (New York: Springer-Verlag, March 2010). He is an author of over 120 journal publications and over 120 conference papers.

Dr. Djordjevic serves as an Associate Editor for the *International Journal of Optics*. Dr. Djordjevic is the Optical Society of America (OSA) member.